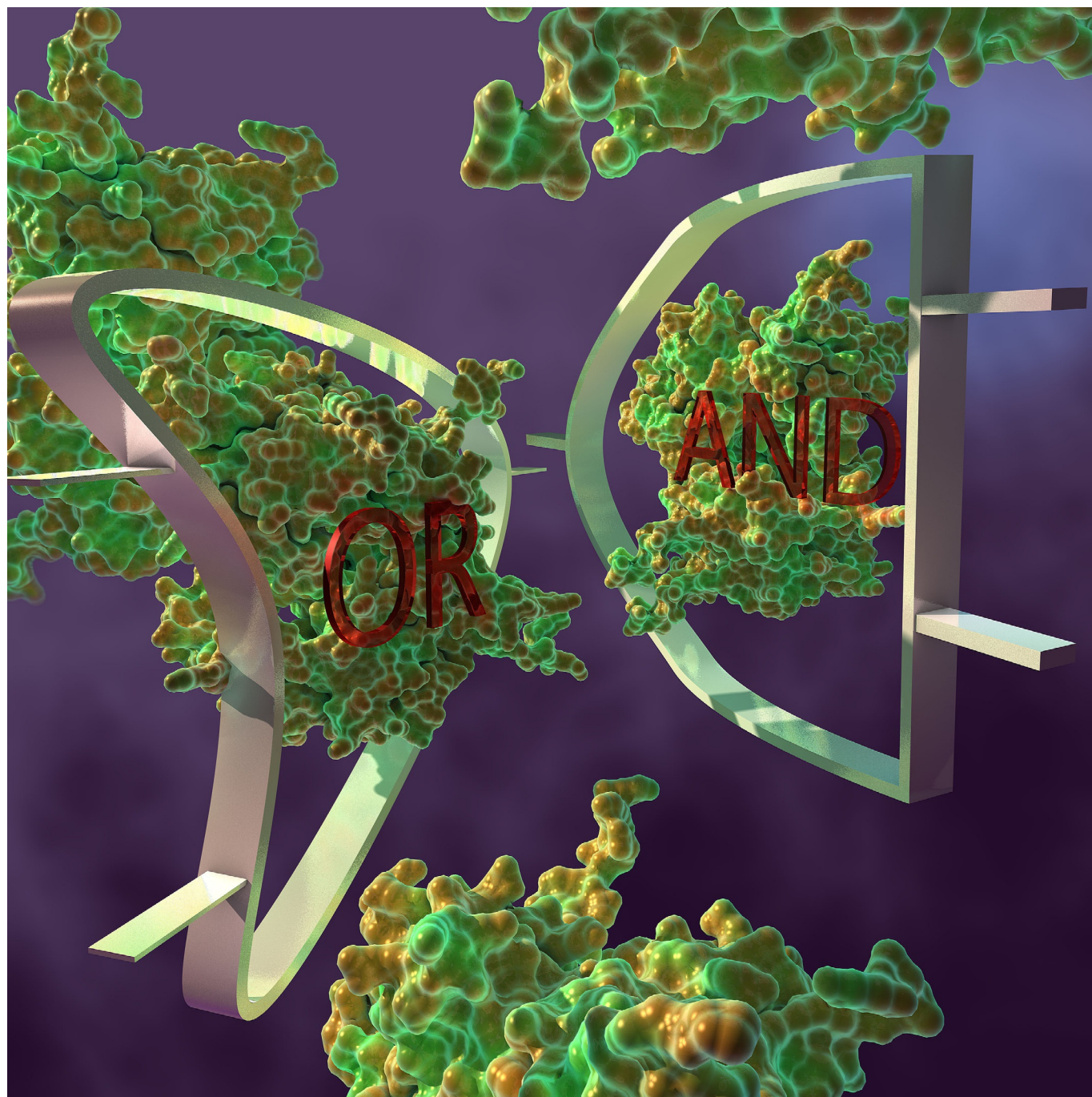


VIP Very Important Paper

Special  
Issue

# Enzyme-Based Logic Gates and Networks with Output Signals Analyzed by Various Methods

Evgeny Katz<sup>\*[a]</sup>



The paper overviews various methods that are used for the analysis of output signals generated by enzyme-based logic systems. The considered methods include optical techniques (optical absorbance, fluorescence spectroscopy, surface plasmon resonance), electrochemical techniques (cyclic voltammetry, potentiometry, impedance spectroscopy, conductivity measurements, use of field effect transistor devices, pH measurements), and various mechanoelectronic methods (using atomic force microscope, quartz crystal microbalance). Although each of the methods is well known for various bioanalytical applications, their use in combination with the biomolecular logic systems is rather new and sometimes not trivial. Many of the discussed methods have been combined with the

use of signal-responsive materials to transduce and amplify biomolecular signals generated by the logic operations. Interfacing of biocomputing logic systems with electronics and "smart" signal-responsive materials allows logic operations be extended to actuation functions; for example, stimulating molecular release and switchable features of bioelectronic devices, such as biofuel cells. The purpose of this review article is to emphasize the broad variability of the bioanalytical systems applied for signal transduction in biocomputing processes. All bioanalytical systems discussed in the article are exemplified with specific logic gates and multi-gate networks realized with enzyme-based biocatalytic cascades.

## 1. Introduction

Recent research in unconventional computing,<sup>[1]</sup> stimulated by the quest for novel ideas potentially breaking limits<sup>[2–5]</sup> of presently used silicon-based technology, resulted in rapid progress in the design of molecular<sup>[6–17]</sup> and biomolecular<sup>[18–25]</sup> logic systems operating as elements of future (bio)molecular computers.<sup>[26]</sup> The logic systems based on synthetic molecules with signal-switchable functionality,<sup>[11,13]</sup> supramolecular systems and molecular machines,<sup>[27]</sup> as well as molecular-functionalized nanospecies,<sup>[28]</sup> have already reached high complexity. The use of biomolecular systems,<sup>[18]</sup> benefiting from their natural specificity in response to chemical input signals and complementarity allowing for easy assembly, brought the research area to an even higher level of sophistication. Biomolecular systems of various composition, based on DNA/RNA,<sup>[22,23,29,30]</sup> oligopeptides,<sup>[31]</sup> proteins/enzymes,<sup>[24,25,32]</sup> and even whole biological cells,<sup>[33–35]</sup> capable of operating in a biological environment,<sup>[36]</sup> have been designed for various logic operations,<sup>[22,24]</sup> performing simple computational operations,<sup>[37–41]</sup> and for being a part of "smart" signal-responsive systems,<sup>[42]</sup> logic functional devices,<sup>[43–46]</sup> and binary YES/NO-operating biosensors.<sup>[47,48]</sup> Research on molecular and biomolecular logic systems is mostly concentrated on the formulation of various logic functions ranging from relatively simple Boolean gates<sup>[49–51]</sup> to very sophisticated multi-input/multi-output gates performing reversible logic operations.<sup>[52–57]</sup> Assembling of individual logic gates in concatenated logic cascades<sup>[58–61]</sup> and complex branching networks<sup>[56,57,62]</sup> is a chemical analogue to designing of computer hardware. Reconfigurable logic gates,<sup>[63–66]</sup> allowing for different computing functions using the same chemical devices, resemble programmable computing operations, thus dem-

onstrating analogy with computer software. However, the analysis of the chemical output signals generated by the biomolecular logic systems is often limited to very few techniques, being mostly represented by optical analysis of the chemical products. Interfacing of biomolecular logic systems with different biosensing, signal-reading, devices attracts little attention of researchers working with biomolecular computing systems. Future progress in the design of biomolecular logic systems, particularly extrapolating this research to the futuristic "molecular computers"<sup>[67]</sup> will certainly require integration of the molecular signal-processing systems with various output-reading devices and methods. Some progress in this direction has been achieved in the recent research, particularly in integrating biomolecular logic systems with electrochemical interfaces<sup>[68]</sup> and signal-responsive materials.<sup>[69]</sup> The present review article overviews different methods of reading output signals generated by biocomputing systems *in vitro*, including various optical, electrochemical/electronic and (nano)mechanical methods. Although the importance of these methods for analysis of different biomolecules, for example DNA, generated by different biocomputing systems should not be underestimated, this paper is concentrated on enzyme-based logic systems, which represent the major scientific interest and research experience of the author. Therefore, most of the logic gates and signal-processing systems discussed in this review originate from the work performed with the contribution of the author of the present article, thus representing his personal experience and scientific vision. Broader visions of the research area of the enzyme logic systems and their applications in unconventional biomolecular computing can be found in many publications originating from other laboratories,<sup>[70–96]</sup> as well as in a recently published book representing various results obtained by leading experts in the area.<sup>[18]</sup> While the present article is a general overview of previously published results, emphasizing the output signal transduction methods, some of the exemplified logic gates were experimentally realized for this paper, thus representing new results.

[a] Prof. E. Katz

Department of Chemistry and Biomolecular Science  
Clarkson University, Potsdam, NY 13699 (USA)  
E-mail: ekatz@clarkson.edu  
Homepage: <http://people.clarkson.edu/~ekatz/>

 The ORCID identification number(s) for the author(s) of this article can be found under: <https://doi.org/10.1002/cphc.201601402>.

 An invited contribution to a Special Issue on Molecular Logic

## 2. General Definitions and Approaches Used in the Realization of Enzyme-Based Logic Systems

Chemical reactions, including those used in biomolecular computing, are not digital by their nature. To digitalize these chemical processes, two levels of concentrations of chemical reacting species are considered as input signals. Logic input **0** is usually considered as the absence of the reacting species, meaning physically zero concentration, whereas logic input **1** could be any experimentally convenient initial concentration of the reacting species that is significantly different from zero. This concentration is usually set by the nature of the biochemical reactions and strongly depends on the technique used for the analysis of the produced chemicals. In the enzyme-based logic systems the input signals could be represented by low molecular weight substrates, which are converted into products in reactions biocatalyzed by enzymes. In this case the substrates are applied at two different concentration levels corresponding to the logic **0** and **1** inputs (again, remember that logic **0** input often corresponds to the physically zero concentration). The chemical inputs are applied in different binary combinations, for example, **0;0**; **0;1**; **1;0** and **1;1** in case of two-input systems. In case of multi-input systems, operating with more than two inputs, the number of variants will be more than four. All other biochemical species, including cofactors, enzymes, and other components of the reacting solutions, are used at the same non-variable initial concentrations, being considered as the "machinery" part of the computing system.<sup>[24]</sup> In some systems, enzymes might be immobilized, whereas the reacting species should always be in a soluble state.<sup>[40,56,57]</sup> On the other hand, enzymes can be used at variable concentrations and considered as logic input signals and applied to a "soup" of substrates/cofactors used at their con-

stant initial concentrations and being ready for reactions in the presence of the enzymes.<sup>[97]</sup> Given that the initial reactants (input signals) are applied at two significantly different concentrations, the products generated after specific reaction time also appear at different concentrations depending on the binary combinations of the used inputs and on the logic implemented in the reaction process. In most of the designed logic systems the output signals represented by the produced chemicals appear at two concentration levels (low and high) defined as logic **0** and **1** outputs, respectively. Various logic gates and networks composed of concatenated logic gates can be realized by selecting different combinations of enzymes and reacting species. In other words, the logic Boolean function connecting the output and input signals can vary depending on the biochemical reactions realized. In some logic systems related to processing naturally appearing biomolecular species the logic input **0** can be different from physically zero concentration. In this kind of biocomputing system the logic **0** and **1** inputs are set by biological processes. In case of biomedical applications of logic gates, **0** and **1** inputs can be defined as normal physiological and pathophysiological concentrations, respectively.<sup>[47,48]</sup> This can significantly complicate analysis of the output signals because they may appear at concentrations with a relatively small difference. Still for the Boolean binary logic, the output signals have to be digitized. The state-of-the-art in the assembling different logic systems has been overviewed in review articles<sup>[24,25]</sup> and book chapters,<sup>[98,99]</sup> thus the present review article does not discuss in details the way to assemble the logic systems, but concentrates on the methods available to analyze the produced logic output signals.

## 3. Optical Analysis of the Output Signals Generated by Enzyme Logic Systems

Optical analysis of chemical products in enzyme-biocatalyzed reactions is frequently used in standard enzyme assay tests, particularly for the assay of enzymatic reactions biocatalyzed by NAD<sup>+</sup>/NADH-dependent dehydrogenases (e.g., lactate dehydrogenase; LDH), oxidases (e.g., glucose oxidase; GOx) or peroxidases (e.g., horseradish peroxidase; HRP).<sup>[100]</sup> The LDH-biocatalyzed production or oxidation of NADH (note that the reaction is reversible) can be easily followed by measuring optical absorbance at  $\lambda=340\text{ nm}$  characteristic of NADH.<sup>[101]</sup> The same optical analysis can be performed for the reaction biocatalyzed by any other NAD<sup>+</sup>/NADH-dependent enzyme. The GOx-biocatalyzed glucose oxidation can be analyzed through the analysis of the concomitant product H<sub>2</sub>O<sub>2</sub>.<sup>[102]</sup> This reaction is usually coupled to the HRP-biocatalyzed formation of a colored product in the presence of H<sub>2</sub>O<sub>2</sub>.<sup>[103]</sup> The chromogenic substrates used in the HRP reaction are usually 2,2'-azino-bis(3-ethylbenzothiazoline-6-sulfonic acid) (ABTS), resulting in the oxidized colored product (ABTS<sub>ox</sub>) absorbing light at  $\lambda=420\text{ nm}$ , or 3,3',5,5'-tetramethylbenzidine (TMB), which is converted into the oxidized product absorbing light at  $\lambda=650\text{ nm}$ . The optical analysis of the ABTS or TMB oxidation products can be used to follow any biocatalytic reaction result-

Evgeny Katz received his Ph.D. in Chemistry from the Frumkin Institute of Electrochemistry (Moscow) in 1983. He was a senior researcher at the Institute of Photosynthesis (Pushchino), Russian Academy of Sciences (1983–1991), a Humboldt fellow at the Technische Universität München (Germany) (1992–1993), and a research associate professor at the Hebrew University of Jerusalem (1993–2006). Since 2006 he is Milton Kerker Chaired Professor at the Department of Chemistry and Biomolecular Science, Clarkson University, NY (USA). He has (co)authored over 430 papers in the areas of biocomputing, bioelectronics, biosensors and biofuel cells. Thomson Reuters included him in the list of the world's top 100 chemists over the past 10 years as ranked by the impact of their published research. Professor Katz was also included in the list of top cited chemists prepared by the Royal Society of Chemistry, with a worldwide rank 378 based on his Hirsch-index, which is currently 83.



ing in the formation of  $\text{H}_2\text{O}_2$  when it is coupled to the process biocatalyzed by HRP. Optical analysis of ATP, can be performed by using the bioluminescence produced by the luciferase/luciferin biocatalytic system.<sup>[104]</sup> Light emission produced by this system is a simple way to analyze ATP, which can be coupled to any other biocatalytic reaction producing or consuming ATP utilized in enzyme logic gates. In the sections below the optical absorbance and bioluminescence assay coupled to biocatalytic reactions mimicking various Boolean logic gates are discussed. Other optical methods, for example, surface plasmon resonance, can be used to follow biocatalytic reactions and analyze the output signals produced by the enzyme logic gates.

### 3.1. Optical Absorbance Measurements for Transduction of Output Signals Produced by the Enzyme Logic Gates

Various enzyme-catalyzed reactions have been used to mimic basic Boolean logic operations with the output signals measured as optical absorbance changes due to formation or consumption of colored biochemicals, including AND,<sup>[105–109]</sup> OR,<sup>[97,109,110]</sup> NAND,<sup>[111]</sup> NOR,<sup>[109,111]</sup> XOR,<sup>[97,109,112,113]</sup> INHIBIT,<sup>[97,109]</sup> Identity,<sup>[109]</sup> and Inverter<sup>[109]</sup> gates. The individual logic gates with the optical absorbance readout have been assembled to form logic networks of different structures and various complexity.<sup>[58,59]</sup> Even more complex multi-enzyme/multi-logic gate branched network with switchable logic operation and optical readout has been applied for analysis of injury biomarkers.<sup>[114]</sup> This system represented the most sophisticated logic network still operating in a single solution. Given that many enzymes operated together performing different logic functions, the optimization of the reacting conditions was extremely complex. This work was extended to reversible logic gates composed of several Boolean operations organized in the form of complex networks: Feynman (Controlled-NOT; CNOT) gate,<sup>[55]</sup> Double Feynman gate,<sup>[56]</sup> Toffoli gate,<sup>[56]</sup> Peres gate<sup>[56]</sup> and Fredkin (Controlled-Swap) gate.<sup>[57]</sup> These logic gates include many enzyme-catalyzed reactions organized in flow systems with

modular architecture allowing for the optical analysis of multiple products in different channels. It should be noted that systems of such high complexity cannot be assembled in a homogeneous solution because of “cross-talking” between different logic gates. Thus, spatial separation of the reacting processes and time difference between them (“clocking”) are mandatory for their realization in flow devices composed of separate reacting cells and channels. Furthermore, the multi-channel design of the logic systems allowed the use of the same chemical species (e.g., NADH) for different logic outputs analyzed separately in different channels. In this section we will discuss example systems of limited complexity based on the enzyme-catalyzed reactions mimicking OR, AND, and XOR logic gates with the output signals measured as optical absorbance changes. More complex systems based on the same optical absorbance readout method are presented in many published papers.<sup>[58,59,114]</sup>

The OR gate was realized by using two parallel biocatalytic reactions activated with two different input signals and producing the same chemical in both reactions considered as the output signal (Figure 1 A). Two enzymes, glucose dehydrogenase (GDH) and alcohol dehydrogenase (ADH), and the NAD<sup>+</sup> cofactor represented the non-variable part of the system (“machinery”), which was the same for all combinations of the applied inputs. Glucose (Glc) and ethanol (EtOH) were defined as input signals, Input A and Input B, respectively, and they were applied to the gate “machinery” in four different combinations: 0,0; 0,1; 1,0 and 1,1, where logic value 0 corresponded to the absence of the input chemical (meaning its zero concentration), and the input concentration corresponding to logic value 1 was optimized experimentally to produce conveniently high output signals. Input A (Glc) was converted into the oxidized product, gluconic acid (GlcA), reducing in the concomitant reaction NAD<sup>+</sup> to yield NADH. This reaction was catalyzed by GDH. In another reaction catalyzed by ADH, EtOH was oxidized to acetaldehyde (Ald) and NAD<sup>+</sup> was reduced to NADH. Overall, NADH, considered as the final output product, was

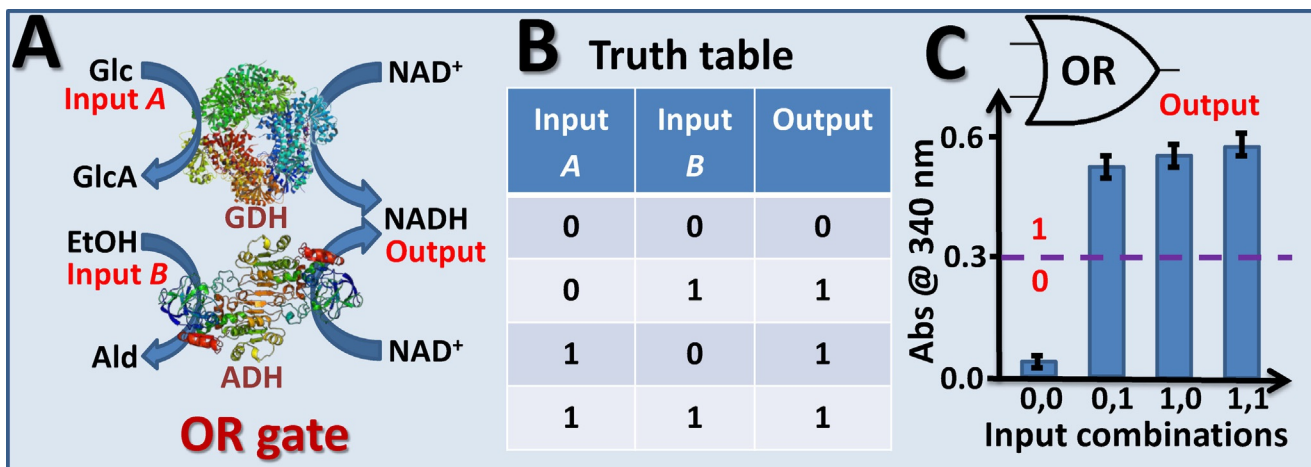


**Figure 1.** Optical absorbance measurements used for analysis of the output signals produced by the enzyme logic gate. A) The OR logic gate based on enzyme catalytic reactions—schematics. Abbreviations used in the scheme are explained in the list of abbreviations. B) Truth table of Boolean OR gate. C) Optical absorbance corresponding to the biocatalytically produced NADH measured for different input combinations. The dash line shows the threshold value separating logic 1 and logic 0 output signals.

produced in the presence of either a single input or both inputs (input combinations 0,1; 1,0 and 1,1). The only input combination resulting in no production of NADH was 0,0 (in other words the absence of both substrates for the biocatalytic reactions). Figure 1B, shows the Truth table corresponding to the OR gate and Figure 1C, shows the experimental results for the enzyme-based system mimicking OR gate function. Note that the biocatalytically produced NADH was analyzed by following optical absorbance at  $\lambda=340$  nm, characteristic of NADH. The low and high absorbance separated by a threshold was considered as 0 and 1 output signals.

The AND gate was realized by using two consecutive biocatalytic reactions activated with two input signals represented by Glc and ABTS, Input A and Input B, respectively (Figure 2A). The “machinery” part of the logic gate included glucose oxidase (GOx) and horseradish peroxidase (HRP); oxygen dissolved in the solution was also present in the system. Glc oxidation and O<sub>2</sub> reduction yielding H<sub>2</sub>O<sub>2</sub> was catalyzed by GOx. The in situ produced H<sub>2</sub>O<sub>2</sub> reacted with HRP, resulting in the biocatalyzed oxidation of ABTS yielding the colored ABTS<sub>ox</sub> product. The two-step biocatalytic process yielded the final ABTS<sub>ox</sub> product, considered as the output signal, only in the

presence of both reacting input species (1,1 input combination). If either or both of the input chemicals were missing (input combinations 0,0; 0,1 and 1,0), the biocatalytic reaction did not proceed to the end and ABTS<sub>ox</sub> was not produced. The biocatalytic process was mimicking the AND logic gate, in which the optical absorbance at  $\lambda=420$  nm characteristic of ABTS<sub>ox</sub> was considered as the output signal. Figure 2B shows the Truth table characteristic of the AND logic operation, and Figure 2C shows the experimental realization of the AND logic gate with the output signals measured optically.

The XOR gate was realized by using two biocatalytic reactions driven in the opposite directions by two input signals represented by Glc and pyruvate (Pyr), Input A and Input B, respectively. The “machinery” part of the logic gate included GDH and lactate dehydrogenase (LDH) (Figure 3A). NAD<sup>+</sup> and NADH cofactors (oxidized and reduced forms, respectively) were added to the system in equal concentrations as a part of the “machinery”. In the presence of Glc, the reaction catalyzed by GDH resulted in the reduction of NAD<sup>+</sup>, thus increasing the NADH concentration and the corresponding absorbance at  $\lambda=340$  nm. On the other hand, in the presence of Pyr, the reaction catalyzed by LDH resulted in the oxidation of NADH, thus

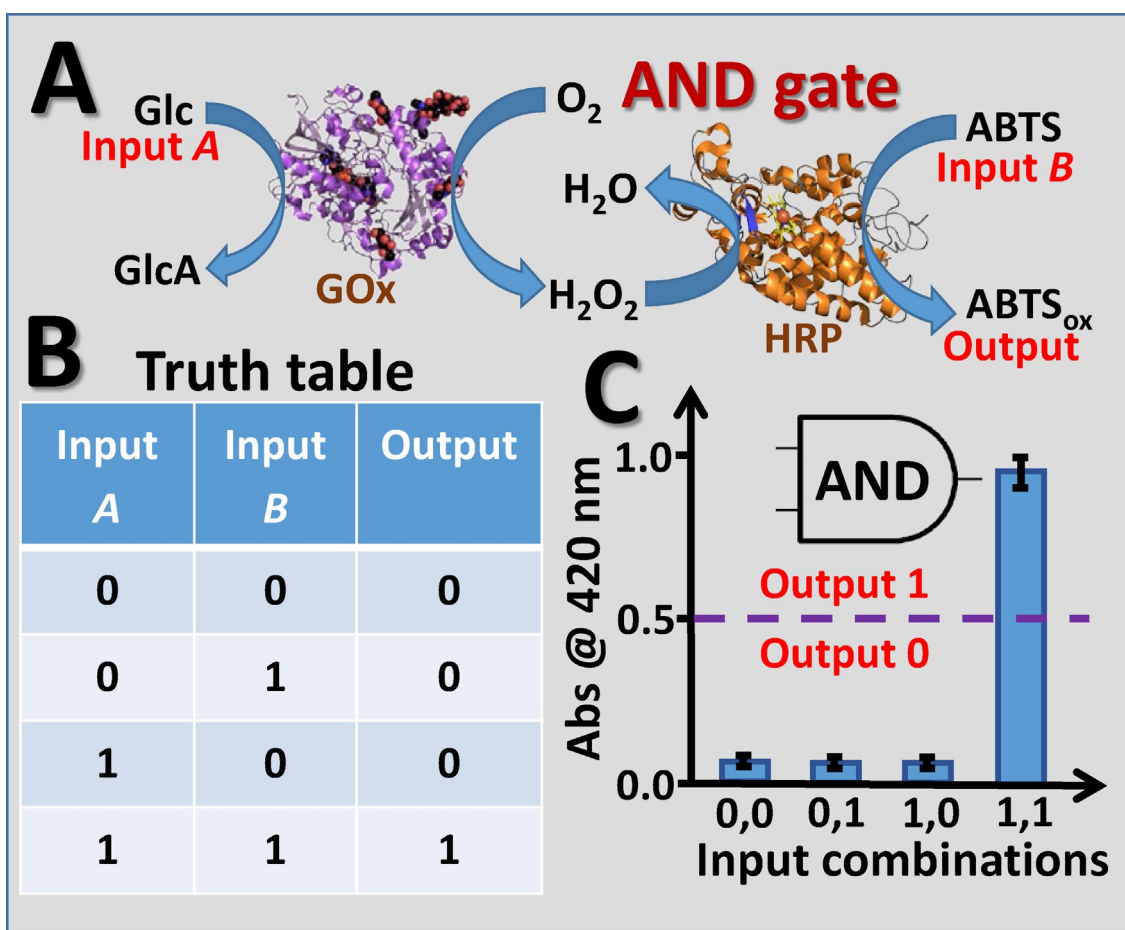


**Figure 2.** Optical absorbance measurements used for analysis of the output signals produced by the enzyme logic gate. A) The AND logic gate based on enzyme catalytic reactions—schematics. Abbreviations used in the scheme are explained in the list of abbreviations. B) Truth table of Boolean AND gate. C) Optical absorbance corresponding to the biocatalytically produced ABTS<sub>ox</sub> measured for different input combinations. The dash line shows the threshold value separating logic 1 and logic 0 output signals.

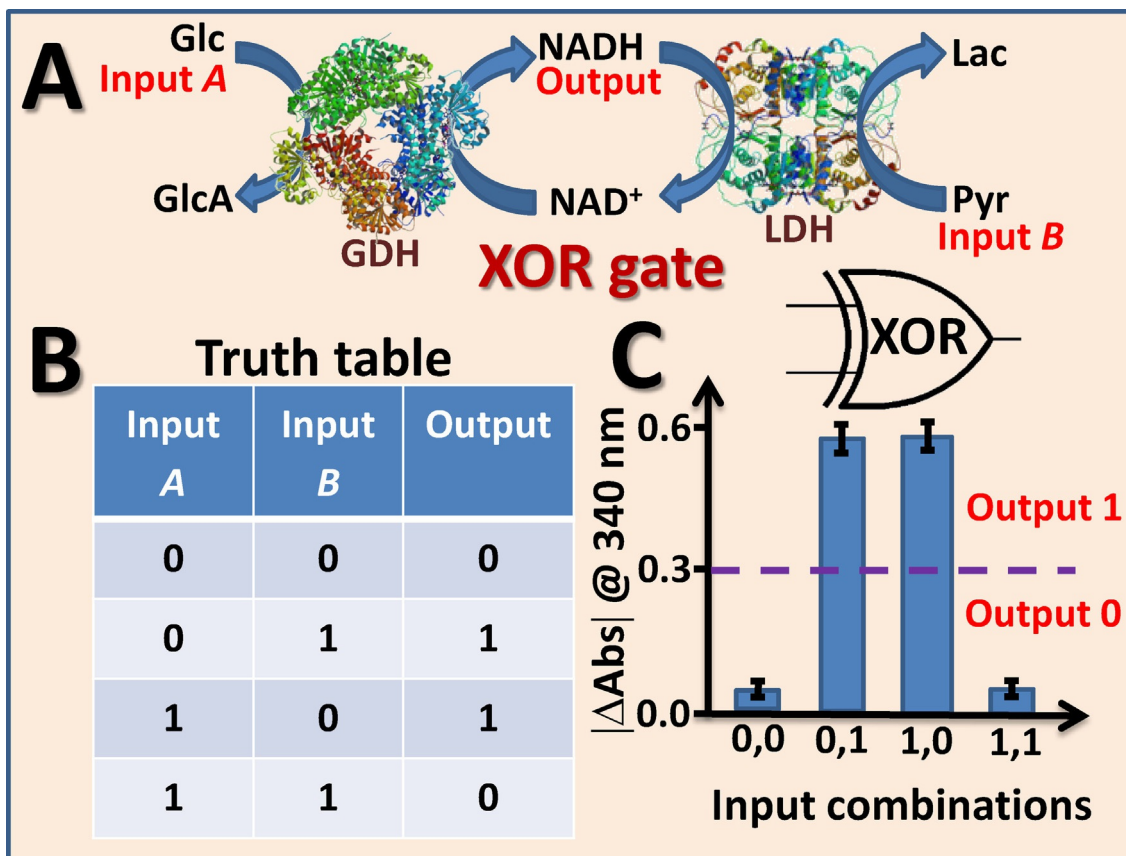


**Figure 3.** Optical absorbance measurements used for analysis of the output signals produced by the enzyme logic gate. A) The XOR logic gate based on enzyme catalytic reactions—schematics. Abbreviations used in the scheme are explained in the list of abbreviations. B) Truth table of Boolean XOR gate. C) Absolute value of the optical absorbance changes corresponding to the biocatalytically produced/consumed NADH measured for different input combinations. The dash line shows the threshold value separating logic 1 and logic 0 output signals.

decreasing its absorbance. Thus, the optical absorbance was changed, increased or decreased, in the presence of Glc or Pyr (input signal combinations 0,1; 1,0), respectively. The biocatalytic reactions were optimized in such a way that both of them running simultaneously (inputs 1,1) compensated each other, thus resulting in no absorbance changes. Clearly, applying no chemical inputs (inputs 0,0) the biocatalytic reactions were not activated and the absorbance was not changed. To fit the XOR gate logic function, the output signal was defined as the absolute value of the absorbance change corresponding to either increase or decrease of the NADH concentration. Figure 3B shows the Truth table of the XOR gate and Figure 3C demonstrates results for its experimental realization. Note that the exemplified XOR gate produces the output signal 0 for the balanced input signals (0,0 and 1,1), whereas the unbalanced inputs (0,1 and 1,0) result in the output 1 measured as the absolute value of the absorbance change.

The three logic gates discussed above are the most typical examples of the enzyme-based systems used for mimicking Boolean logic operations. Many other gates with different logic<sup>[109]</sup> and more complex signal processing functions<sup>[55–57]</sup> have been experimentally realized by using optical absorbance measurements as the transduction technique to follow the output signals.

A different approach to the optical analysis of output signals produced by the enzyme logic gates was realized by using the shift of the absorbance band rather than change of the absorbance intensity.<sup>[115]</sup> The optical analysis was based on the dependence of plasmon energy in Au nanostructures controlled by the electrical charge formed on their surfaces. Magnetic-core ( $\text{CoFe}_2\text{O}_4$ )-Au-shell nanoparticles (NPs;  $18 \pm 3 \text{ nm}$ )<sup>[116]</sup> were functionalized with a thiolated monolayer bearing carboxylic groups (Figure 4A). The charge produced on the surface of the NPs was controlled by the dissociation state of the surface-bound carboxylic groups. At the initial neutral pH the carboxylic groups were dissociated, thus producing a negative charge on the surface. When pH was decreased below the  $pK_a$  of the carboxylic groups (ca.  $5.2 \pm 0.1$ )<sup>[117]</sup> the carboxylic groups were protonated and the surface charge became neutral. This pH-dependent change of the surface charge resulted in a change of the surface-localized plasmon energy, thus shifting the  $\lambda_{\text{max}}$  absorbance band of the NPs (the neutral charge resulted in a shift of the  $\lambda_{\text{max}}$  to longer wavelength—a redshift of the absorbance band). The pH change was produced by the enzyme-catalyzed reactions mimicking OR and AND logic gates.<sup>[115]</sup> The enzymes were covalently bound to  $\text{SiO}_2$  particles (ca.  $74 \mu\text{m}$  diameter) used as a platform for the biocatalysts. Figure 4A shows schematically the biocatalytic process mim-

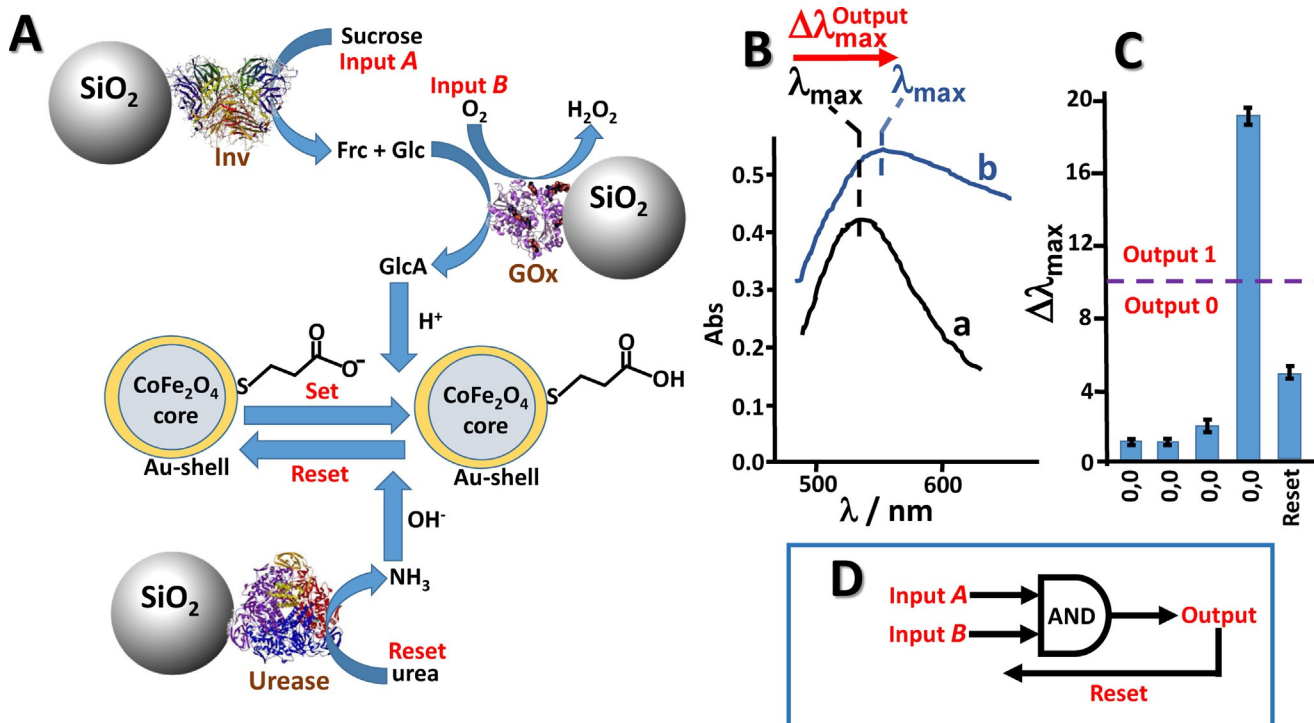


**Figure 4.** Optical absorbance measurements used for analysis of the output signals produced by the enzyme logic gate. A) The AND-Reset logic system based on the biocatalyzed reactions and integrated with the magnetic-core/Au-shell nanoparticles functionalized with a thiolated monolayer containing carboxylic groups. Abbreviations used in the scheme are explained in the list of abbreviations. B) Absorbance spectra corresponding to the LSPR of the NPs measured at different pH values: a) pH 7.0, b) pH ca. 4. C) Logic output defined as the  $\lambda_{\text{max}}$  shift generated by the system upon application of various combinations of the input signals and the reset signal. The dash line shows the threshold value separating logic 1 and logic 0 output signals. D) Logic scheme of the AND-Reset system. A fragment of this figure was adapted from ref. [115] with permission.

icking the AND logic gate (the OR gate was mimicked in a similar way but using different enzymes catalyzing different reactions). The biocatalytic process was activated with two inputs, sucrose and O<sub>2</sub>, Inputs A and B, respectively. Sucrose was cut to fructose (Frc) and glucose (Glc) in the reaction catalyzed by invertase (Inv). Then glucose was oxidized by O<sub>2</sub> in the reaction catalyzed by GOx, yielding gluconic acid (GlcA), thus, decreasing the pH value. The two-step biocatalytic reaction proceeded to the end only in the presence of both input signals (logic combination 1,1), thus mimicking the AND logic gate. The in situ produced low pH resulted in the protonation of the surface-confined carboxylic groups and in the absorbance wavelength shift originating from the change of the localized surface plasmon resonance (LSPR) (Figure 4B). The large shift of the  $\lambda_{\text{max}}$  (ca. 20 nm) was observed only for the 1,1 combination of the input signals, whereas  $\lambda_{\text{max}}$  was preserved almost unchanged for all other input combinations (0,0; 0,1; 1,0), as expected for the AND gate (Figure 4C). The logic gate was reset to the initial pH and to almost initial  $\lambda_{\text{max}}$  by the reaction catalyzed by urease converting urea into NH<sub>3</sub> (Figure 4A,C). The whole biocatalytic system represented the two-input AND gate with a Reset function (Figure 4D). Different components of the logic system played different roles in the signal processing and output readout. The SiO<sub>2</sub> particles suspended in the solution operated as a convenient platform for enzyme immobilization, the superparamagnetic core (CoFe<sub>2</sub>O<sub>4</sub>) allowed easy manipulation of the signal-reading NPs in the presence of an external

magnetic field, whereas the Au-shell was the reporting unit transducing pH changes to the optical signals. Other logic systems based on the enzyme-catalyzed pH changes are discussed below in Sections 4.3–4.6.

### 3.2. Bioluminescence Measurements for Transduction of Output Signals Produced by the Enzyme Logic Gates

Although optical absorbance measurements are the most frequently used method for analyzing output signals generated by the enzyme logic systems, the method is limited to processes that yield or consume chemicals that absorb light in the visible (including near-UV) range of wavelength. The use of short-UV or IR spectra are not convenient for multi-component complex biochemical systems (note that proteins/enzymes absorb light around 280 nm, thus restricting optical measurements of the output signals in the UV region). Therefore, analysis of biomolecules that are not colored requires different techniques. The most typical example is bioluminescent analysis of adenosine triphosphate (ATP) through a biocatalytic reaction in the presence of the luciferase/luciferin system.<sup>[104]</sup>

Figure 5 A shows a two-step biocatalytic reaction in the presence of two enzymes, pyruvate kinase (PK) and luciferase (Luc), activated by three inputs, phosphoenol pyruvate (PEP), adenosine diphosphate (ADP), and luciferin (Lucif), Inputs A, B, and C, respectively. The first reaction catalyzed by PK results in the consumption of PEP and the concomitant conversion of ADP

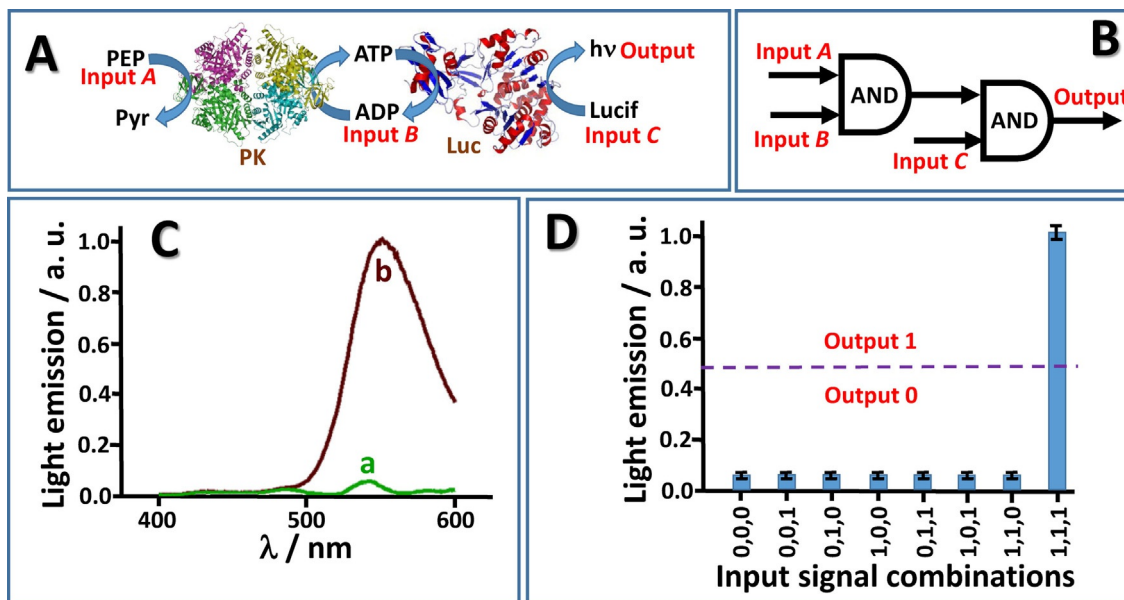


**Figure 5.** Bioluminescence measurements used for analysis of the output signals produced by the enzyme logic gate. A) Two concatenated AND logic gates based on enzyme catalytic reactions—schematics. Abbreviations used in the scheme are explained in the list of abbreviations. B) Logic scheme of the concatenated AND gates. C) Bioluminescence spectra measured for the logic system when it produces output 0 (a) and 1 (b). D) Light emission by the bioluminescent system measured for different combinations of the input signals. The dash line shows the threshold value separating logic 1 and logic 0 output signals. A fragment of this figure was adapted from ref. [60] with permission.

into ATP. Then, the second reaction catalyzed by Luc results in bioluminescence when ATP is produced through the first reaction and luciferin is present in the system. The two-step reaction activated with three input signals resembles a logic network composed of two concatenated AND gates (Figure 5B). Indeed, both biocatalytic reactions proceed until the end only in the presence of all reacting species (input combination 1,1,1), whereas the absence of any of the input chemicals should inhibit the bioluminescence. Figure 5C, curve b, shows the light emission spectrum (bioluminescence) defined as the output signal 1 and observed for the input combination 1,1,1. All other input signal combinations resulted in the output signal 0 observed as low intensity background luminescence (Figure 5C, curve a). The bar chart (Figure 5D) shows all experimentally measured output signals for eight combinations of the inputs. The present system exemplifies application of bioluminescence as a method for observing output signals generated in the presence of ATP, which is a very common component of various enzyme-based logic systems of various complexity.<sup>[60]</sup> Another system mimicking a branched logic network was based on bioluminescence produced upon oxidation of luminol catalyzed by horseradish peroxidase (HRP) in the presence of enzymatically produced H<sub>2</sub>O<sub>2</sub>.<sup>[118]</sup> Since H<sub>2</sub>O<sub>2</sub> is a common product of many enzyme reactions (represented by different oxidases, including glucose oxidase, lactate oxidase, etc.), the bioluminescence produced by the H<sub>2</sub>O<sub>2</sub>-HRP-luminol system is a very convenient method of output signal transduction, and it is particularly useful when the absorbance measurements are difficult, for example, in heterogeneous systems.

### 3.3. Surface Plasmon Resonance Measurements for Transduction of Output Signals Produced by the Enzyme Logic Gates

Redox reactions taking place in polymer thin films deposited on a gold surface result in changes in surface reflectance and can be detected by surface plasmon resonance (SPR) measurements.<sup>[119,120]</sup> These surface redox processes can be coupled to biocatalytic reactions<sup>[121,122]</sup> and used to analyze output signals produced by the enzyme-based logic gates. Figure 6A shows schematically the reaction catalyzed by LDH and activated with two input chemicals: lactate (Lac) and NAD<sup>+</sup>, Input A and Input B, respectively. The reaction resulted in the reduction of NAD<sup>+</sup> to NADH with the concomitant oxidation of Lac to pyruvate (Pyr). The biocatalytic system operated in a solution in contact with a chemically modified Au surface (SPR plate). Prussian Blue (PB), an inorganic, insoluble, three-dimensional polymer, was deposited electrochemically on the Au surface and used to transduce the biocatalytic reaction output (NADH) to the surface reflectance changes measured by SPR.<sup>[122]</sup> The processes was started when PB was in the oxidized state, Fe<sub>4</sub><sup>III</sup>[Fe<sup>II</sup>(CN)<sub>6</sub>]<sub>3</sub>, produced by applying 0.3 V (vs. Ag/AgCl reference electrode) on the modified electrode. This state of PB demonstrated a relatively high reflectance measured by SPR method (Figure 6B, curve a). In the presence of the biocatalytically produced NADH, PB was chemically reduced to the K<sub>4</sub>Fe<sub>4</sub><sup>II</sup>[Fe<sup>II</sup>(CN)<sub>6</sub>]<sub>3</sub> state with a smaller reflectance (Figure 6B, curve b); thus, the reflectance value responded to the absence or presence of NADH in the solution. Before any reaction, the modified surface demonstrated a high reflectance corresponding to the initial oxidized state of PB, but the reflectance de-

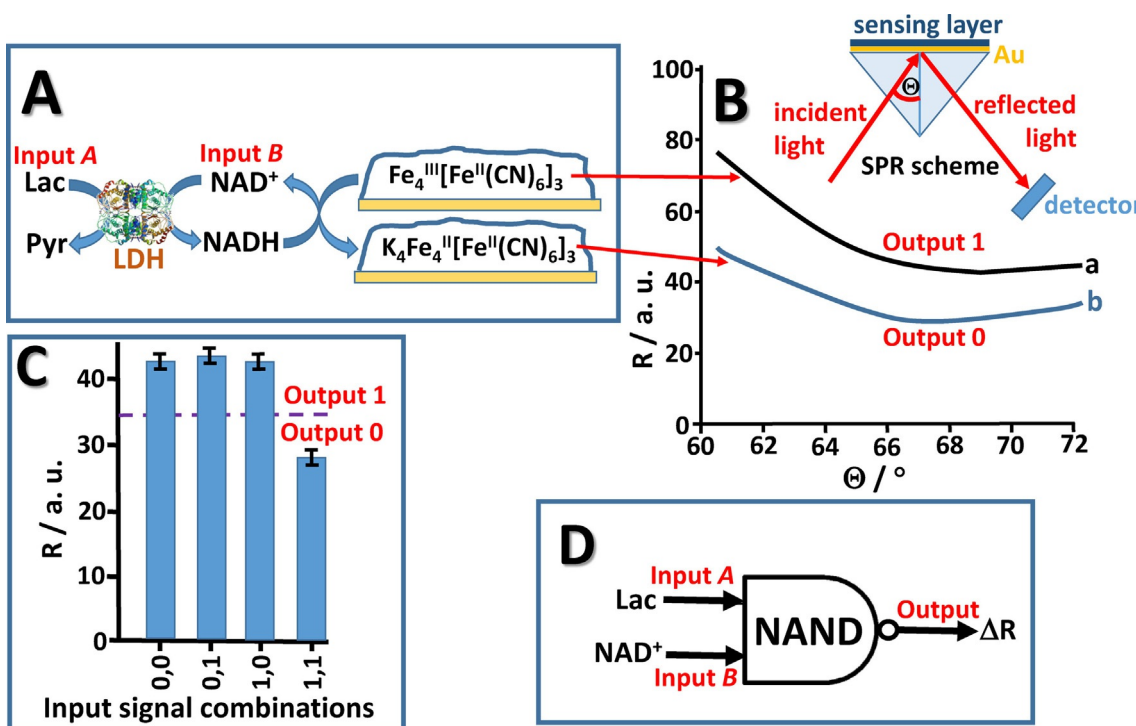


**Figure 6.** SPR measurements used for analysis of the output signals produced by the enzyme logic gate. A) The NAND logic gate based on enzyme catalytic reactions coupled to redox transformations of Prussian Blue thin film on an SPR sensing surface. Abbreviations used in the scheme are explained in the list of abbreviations. B) Reflectance spectra measured by SPR and corresponding to the output 1 (a) and 0 (b). C) Reflectance measured by SPR at  $\Theta = 68^\circ$  for different combinations of the input signals. The dash line shows the threshold value separating logic 1 and logic 0 output signals. D) NAND gate scheme.

creased after the biocatalytic production of NADH due to the formation of the reduced state of PB on the surface. Input A and Input B signals (Lac and NAD<sup>+</sup>) were applied in four different combinations, but the reaction resulted in NADH formation only in the presence of both inputs (1,1 combination). Therefore, the original high reflectance was preserved when the inputs were applied in 0,0; 0,1 and 1,0 combinations and it was decreased in the case of 1,1 combination (Figure 6C). The high reflectance was defined as the output signal 1, whereas the smaller reflectance was considered as the output 0. The function demonstrated by the system resembles a NAND logic gate with the SPR transduction of the output signal (Figure 6D). The SPR transduction of the output signal can be beneficial if the direct optical measurements of NADH are difficult; for example, in the presence of other colored components in the system absorbing light similar to the NADH spectrum.

#### 4. Electrochemical Analysis of the Output Signals Generated by Enzyme Logic Systems

Electrochemical methods can be conveniently applied to the analysis of the output signals produced by the enzyme logic systems when redox-active species (e.g., H<sub>2</sub>O<sub>2</sub> or NADH) are produced or consumed as the result of the logic operations.<sup>[123–125]</sup> The electroanalytical methods used in such applications could be similar to those used in electrochemical biosensors. Various electroanalytical methods, including chronoamperometry<sup>[124,125]</sup> and potentiometry,<sup>[126–128]</sup> can be em-

ployed for detecting the output signals. The potentiometry methods can be extended to the use of ion-selective and pH-sensing electrodes,<sup>[129–131]</sup> thus extending the output signal measurements to the analysis of various species that are not necessarily redox active. Coupling enzyme-catalyzed reactions with switchable stimuli-responsive materials deposited on electrode surfaces allow for indirect electrochemical analysis of the output signals, which are not redox active and not directly detectable by electrochemical means.<sup>[42,68,129–135]</sup> For example, pH variation in the course of the enzyme-catalyzed reactions mimicking logic operations have been used to activate electrodes functionalized with pH-switchable polymer-based thin films. The pH changes produced by the biocatalytic system resulted in switching of a polymer-brush thin film between a non-permeable shrunk state and a permeable swollen state, thus allowing the electrochemical analysis of the interfacial state using cyclic voltammetry or impedance spectroscopy.<sup>[130,131]</sup> Based on the same concept, but using a pH-switchable nanoporous membrane deposited on an electrode surface, enzyme logic operations were transduced to electrical outputs by impedance spectroscopy.<sup>[136]</sup> Notably, in these systems the electrochemical analysis was used to follow the interfacial properties of the modified electrode rather than direct analysis of the chemical species produced by the enzyme reactions. Signal-switchable materials can be used not only as thin films on sensing electrodes, but also as switchable components of a bulk liquid phase; for example, in the form of a micro-emulsion switchable between oil-in-water and water-in-oil states.<sup>[137]</sup>

This system can be switched between the states with the low and high electrical resistance upon getting signals produced by an enzyme logic gate. The change in the system state can be followed by using simple DC-electrical conductivity measurements. In addition to electrochemical measurements on conducting electrodes, semiconducting devices (usually in the form of field-effect transistors, FET) have been used for electronic transduction of chemical output signals produced by enzyme logic systems.<sup>[138–143]</sup>

#### 4.1. Chronoamperometric Transduction of Chemical Output Signals Produced by the Enzyme-Based Logic Systems

Figure 7 exemplifies use of chronoamperometric measurements for analysis of the output signals produced by the enzyme logic system.<sup>[125]</sup> The biocatalytic cascade was initiated by glutamate (Glu) and glucose dehydrogenase (LDH), Input A and Input B, respectively. Note that in this hybrid system one of the inputs was represented by a substrate for an enzymatic reaction (Glu), and the second input was an enzyme (LDH) (Figure 7A). Two other enzymes, glutamate oxidase (GluOx) and alanine transaminase (ALT), as well as required substrates, alanine (Ala), NADH and O<sub>2</sub>, were non-variable parts of the logic gate ("machinery"). Both inputs used in the logic system were represented with biomarkers of traumatic brain injury (TBI), thus aiming at the logic processing of the biomarker concentration changes and TBI diagnosis. In this biomedical/bioanalytical application, the logic values 0 and 1 of the input signals were defined as their physiologically normal and elevated pathophysiological concentrations, respectively. The multistep

biocatalytic reaction (Figure 7A) used in the logic analysis of the input signals (biomarkers) proceeded at any combination of the inputs because the logic 0 was not physically zero concentration of the reacting species. However, the rate of the process was strongly dependent on the logic combination of the input signals reflecting a difference in their concentrations. The highest rate of the biocatalytic reaction was achieved at 1,1 combination of the inputs, whereas all other combinations (0,0; 0,1 and 1,0) resulted in low rates of the biocatalytic reactions. The output signal was defined as the current on a sensing glassy carbon electrode corresponding to electrochemical oxidation of NADH. Since the analyzed species was consumed (not produced) by the biocatalytic reaction, the output signal was smaller for the higher concentrations of the input species, thus representing the NAND gate (Figure 7B). The biocatalytic reaction was allowed for six minutes after adding the input signals to the gate "machinery" and then the chronoamperometric analysis of the residual NADH was performed. Figure 7C shows the experimental chronoamperometric current changes obtained at different logic combinations of the inputs and Figure 7D shows the current values measured after 15 seconds of chronoamperometric measurements. The low output signal (logic value 0) obtained at 1,1 combination of the inputs was signaling on the TBI conditions, thus allowing biomedical diagnosis based on the combined consideration of both TBI biomarkers. Despite the fact that the logic analysis of the biomarkers was performed in a model system, the developed approach holds promise for future rapid diagnostics of TBI in the binary "YES/NO" format, which is particularly useful for point-of-care applications.

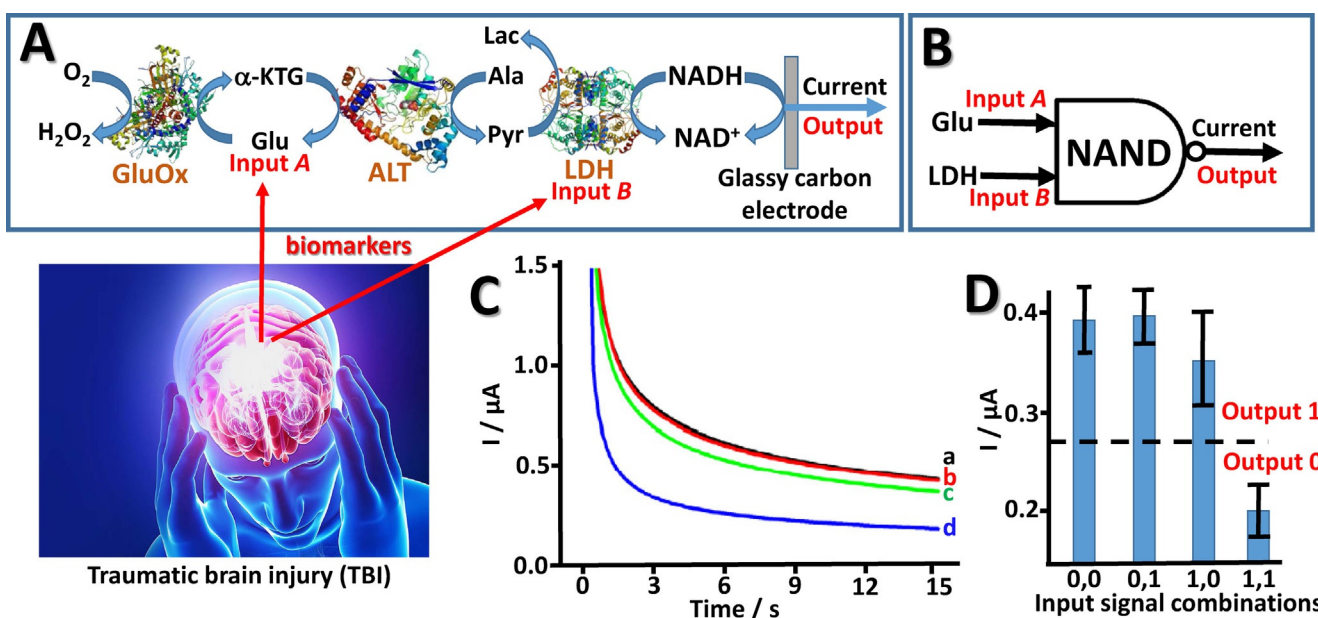


**Figure 7.** Electrochemical transduction of the enzyme generated output signals—chronoamperometric measurements. A) The NAND logic gate based on enzyme catalytic reactions with the input signals corresponding to traumatic brain injury (TBI) biomarkers. NADH participating in the biocatalytic process is analyzed by chronoamperometry (at  $-0.1$  V vs. Ag/AgCl) on a glassy carbon electrode. Abbreviations used in the scheme are explained in the list of abbreviations. B) NAND gate scheme. C) Chronoamperometric curves measured for different combinations of the input signals. D) Current measured by chronoamperometry after 15 sec from the beginning of the potential step for different combinations of the input signals. The dash line shows the threshold value separating logic 1 and logic 0 output signals. A fragment of this figure was adapted from ref. [125] with permission.

#### 4.2. Potentiometric Transduction of Chemical Output Signals Produced by the Enzyme-Based Logic Systems

Electrochemical analysis of NADH participating in biocatalytic reactions can be performed by different electrochemical methods, including potentiometric measurements (Figure 8). An example system,<sup>[127]</sup> represented by a biocatalytic cascade activated with four input signals (Figure 8A), mimicked three concatenated AND logic gates (Figure 8B). The biocatalytic process proceeded to the end only if all input signals appeared at the logic values 1 (1,1,1,1 combination), thus resulting in the formation of NADH as the final product. The sensing electrode was modified with pyrroloquinoline quinone (PQQ), which is a known catalyst for the NADH oxidation.<sup>[144]</sup> The electrocatalytic oxidation of NADH on the PQQ-modified electrode can proceed spontaneously (this was used previously in biofuel cells based on NADH oxidation)<sup>[145,146]</sup> resulting in the forma-

tion of the negative potential measured vs. a reference electrode (RE). Figure 8C shows the potential produced on the PQQ-modified sensing electrode at different combinations of the variable logic inputs (16 variants), for which only one input combination (1,1,1,1) resulted in the high negative potential corresponding to the NADH production in the biocatalytic cascade, as expected for the system mimicking three concatenated AND gates. Similar potentiometric measurements have been used for transduction of NADH formation to the electronic output in other logic systems of high complexity.<sup>[126]</sup>

#### 4.3. pH-Measurements as a Tool for Transduction of Chemical Output Signals Produced by the Enzyme-Based Logic Systems

Many enzyme-catalyzed processes produce acids or bases upon redox or hydrolytic reactions. Typical examples are for-

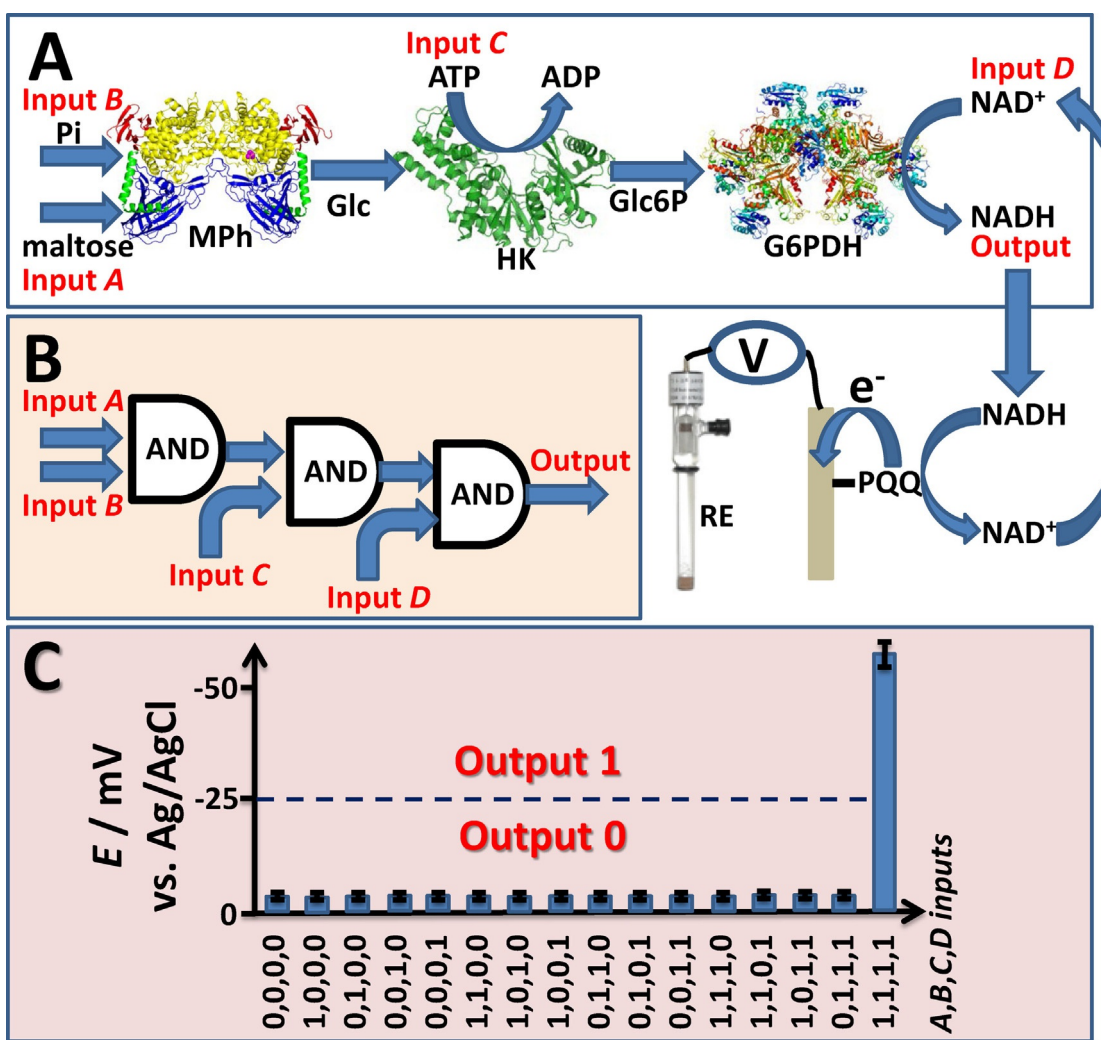


**Figure 8.** Electrochemical transduction of the enzyme generated output signals—potentiometric measurements. A) The biocatalytic cascade activated with four input signals and ended with the reduction of  $\text{NAD}^+$  to NADH. The produced NADH was analyzed potentiometrically on an electrode modified with PQQ catalyzing its oxidation. The negative potential produced on the PQQ-sensing electrode in the presence of NADH was measured vs. a reference electrode. Abbreviations used in the scheme are explained in the list of abbreviations. B) The logic scheme composed of three concatenated AND logic gates corresponding to the biocatalytic cascade shown in (A). C) Potentials produced on the PQQ-sensing electrode after applying four input signals in 16 different combinations. The dash line shows the threshold value separating logic 1 and logic 0 output signals. A fragment of this figure was adapted from ref. [127] with permission.

mation of gluconic acid (GlcA) upon oxidation of glucose catalyzed by GOx or GDH, and production of organic acids from esters in reactions catalyzed by esterase. These reactions, if they proceed in a solution with low buffer capacity or without buffer at all, result in bulk pH changes, which can be used to follow the enzymatic reaction and can serve as the final output signal. Enzyme-based logic gates (e.g., OR, AND)<sup>[42,115,129,131,136,147–150]</sup> and logic networks of different complexity<sup>[68,130,147,151]</sup> have been realized by using  $\Delta\text{pH}$  as the output signal measured with a regular pH-sensitive electrode and standard pH-meter. On the other hand, hydrolytic decomposition of urea catalyzed by urease produces ammonia, thus increasing pH value. This reaction can be used to reset the initial neutral pH value after it was decreased by the biocatalytic reactions producing acids.<sup>[136]</sup>

Figure 9A shows a reaction cascade catalyzed by four enzymes operating as a “machinery”, alcohol dehydrogenase (ADH), glucose dehydrogenase (GDH), amyloglucosidase (AGS) and invertase (Inv), activated with four input signals represented by NADH, acetaldehyde (Ald), maltose and sucrose, Inputs A, B, C, and D, respectively.<sup>[147]</sup> The final product of the biocatalytic reactions is gluconic acid (GlcA), which results in acidification of the reaction solution when the reactions proceed to the very end. The pH decrease ( $\Delta\text{pH}$ ) in the bulk solution was considered as the output signal measured with a standard pH-sensing electrode. The reaction cascade included two path-

ways. One was represented by two parallel reactions catalyzed by AGS and Inv and triggered with maltose and sucrose, respectively. This part of the reaction cascade mimics an OR logic gate and results in the production of glucose. The second pathway was composed of two consecutive reactions biocatalyzed by ADH and GDH and activated with Ald and  $\text{NAD}^+$ , respectively. The first reaction step activated with Ald and NADH represents an AND logic gate. The final reaction step, converting glucose into GlcA, was catalyzed by GDH only when both intermediate products,  $\text{NAD}^+$  and glucose, were produced, thus also representing an AND gate connected to the AND-OR gates operating in parallel (Figure 9B). The final output ( $\Delta\text{pH}$ ) was high (meaning logic value 1) only when both intermediate products, glucose and  $\text{NAD}^+$ , were produced through the OR and AND gates. This was achieved at the input logic combinations 1,1,1,0; 1,1,0,1 and 1,1,1,1; otherwise the output signal was 0 (meaning small pH changes for all other input combinations) (Figure 9C). Whereas pH changes can be measured directly in the bulk solution, they can be further used to change interfacial properties of signal-responsive materials associated with electrode surfaces or emulsions, and then analyzed by using different electrochemical methods (not measuring pH changes directly). These systems are overviewed in the next sections.

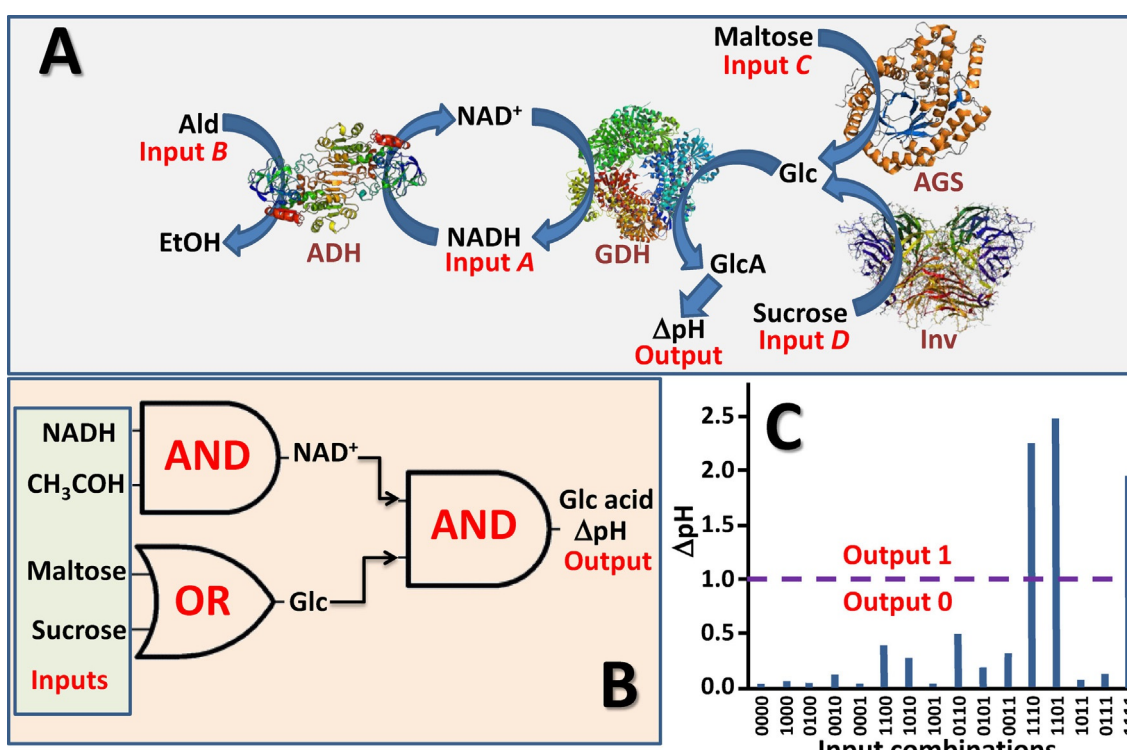


**Figure 9.** Electrochemical transduction of the enzyme generated output signals—pH measurements. A) The biocatalytic cascade activated with four input signals and ended with oxidation of glucose to gluconic acid. The pH change was defined as the output signal measured with a standard pH-sensitive electrode. Abbreviations used in the scheme are explained in the list of abbreviations. B) The equivalent logic network corresponding to the biocatalytic cascade shown in (A). C) Bulk pH changes obtained with different combinations of the logic inputs. The dash line shows the threshold value separating logic 1 and logic 0 output signals. A fragment of this figure was adapted from ref. [147] with permission.

#### 4.4. Indirect Electrochemical Analysis of Output Signals Generated by the Enzyme-Based Logic Systems Using Electrodes Functionalized with pH-Switchable Polymers

Stimuli-responsive materials, exemplified by organic polymers<sup>[152–154]</sup> and more specifically by polyelectrolyte brushes attached to a modified electrode surface,<sup>[155–159]</sup> can be used to analyze electrochemically changes in the environment, particularly variation of the pH value. Indeed, protonation-deprotonation of the polyelectrolyte brushes results in their restructuring between a swollen hydrophilic state, permeable for ionic species of the opposite charge, and collapsed hydrophobic state, which is non-permeable for ionic species, thus inhibiting electrochemical processes at the electrode surface. Various polyelectrolyte brushes have been produced on electrodes and demonstrated pH-switchable electrode activity.<sup>[155–159]</sup> These pH-switchable modified electrodes have been functionally coupled to the enzyme-based logic systems, producing pH changes *in situ* as the output signal of the logic operations.<sup>[68, 130, 131, 151]</sup> Whereas in the majority of the reported systems the enzyme reactions have been performed in solutions, in some structurally advanced assemblies the enzymes were physically bound to the modified electrode surfaces producing local pH changes at the interfaces, thus resulting in the switch of the electrode activity without bulk pH changes.<sup>[160]</sup>

Two important factors should be taken into account when pH-switchable polyelectrolyte brushes are used as stimuli-responsive materials in connection with the pH changes produced by the enzyme logic systems. 1) The range of the pH changes produced by the biocatalyzed reactions should include the  $pK_a$  value of the polyelectrolyte. In other words, the pH change should be enough to change the protonation state of the polymer brushes. 2) The direction of the pH change should correspond to the specific application. For example, decreasing pH upon production of acids (e.g., gluconic acid in the biocatalytic oxidation of glucose) can result in protonation of polyelectrolyte brushes, thus converting them into the positively charged state permeable for anionic redox species, thus activating the modified electrode in the presence of the anionic redox probe. The opposite pH change (possibly in the reset process) can inhibit the electrochemical reactions on the modified electrode surface.

A biocatalytic cascade, outlined schematically in Figure 10A, results in a pH decrease because of the production of GlcA as the final product of a multistep enzyme-catalyzed reaction.<sup>[130]</sup> Three enzymes, alcohol dehydrogenase (ADH), glucose dehydrogenase (GDH), and glucose oxidase (GOx), activated with four input signals: NADH, acetaldehyde, glucose and oxygen, Inputs A, B, C and D, respectively, operate in concert, performing logic operations on the inputs applied in different combinations. Figure 10B explains the biocatalytic reactions in terms of logic operations, in the form of a network composed of four concatenated-branched logic gates. The biocatalytic cascade finally resulting in the pH change was controlled by the pattern of the applied inputs. The pH decrease generated *in situ* by the biochemical reactions was coupled with restructuring of a pH-responsive poly(4-vinyl pyridine)-(P4VP)-brush-functional-

ized electrode. The reorganization of the pH-sensitive P4VP-brush polymer from its neutral and hydrophobic state to the protonated and swollen state resulted in a switch of the electrode interface from the OFF state, when electrochemical reactions are inhibited, to the ON state, when the electrode is electrochemically active (Figure 10C). The ON-OFF switch of the electrode activity was analyzed following an electrochemical reaction of a soluble diffusional redox probe,  $[\text{Fe}(\text{CN})_6]^{3-/4-}$  (Figure 11). This allowed the logic output generated by the enzyme-catalyzed reactions to be analyzed by electrochemical means. Cyclic voltammograms (Figure 11A) and Faradaic impedance spectra (Figure 11C) measured on the P4VP-modified electrode demonstrated its switchable features controlled by the pH value, changed by the enzyme reactions depending on the combinations of the chemical inputs applied to the logic system. Since the number of the variable inputs was four, the whole set of the input signal combinations included 16 variants. The input combinations resulting in the production of GlcA and thus decreasing the pH value were considered to generate the logic output 1. Otherwise, in case of no pH changes because of no production of GlcA, the system generated the output signal 0. The produced pattern of the output signals was determined by the Boolean logic encoded in the logic circuitry (Figures 11B,D). The use of the switchable P4VP-modified electrode controlled by the pH changes allows amplification of the output signals. Indeed, the concentrations of the chemical inputs applied for activating the biocatalytic reactions and concentrations of the biocatalytically produced outputs might be much smaller than the concentration of the redox probe (in the present example  $[\text{Fe}(\text{CN})_6]^{3-/4-}$ ) operating with the switchable electrode. Therefore, the response corresponding to the redox probe measured by electrochemical means in the form of changes in the cyclic voltammograms or Faradaic impedance spectra might be much higher compared with the electrochemical responses measured directly for the biochemical species participating in the enzyme-catalyzed reactions.

#### 4.5. Conductivity Measurements as a Tool for Transduction of Chemical Output Signals Produced by the Enzyme-Based Logic Systems

Signal-responsive materials (specifically, polyelectrolyte brushes) can be associated not only with electrode surfaces, as discussed in the previous section, they can also be integrated with various heterogeneous systems, bringing to them signal-switchable features. For example, silica nanoparticles ( $\text{SiO}_2$ -NPs; 200 nm diameter) were functionalized with polyelectrolyte brushes to allow their switchable hydrophobicity-hydrophilicity features to be controlled by external pH changes generated by enzymatic reactions.<sup>[137, 161]</sup> Figure 12A shows reactions resulting in the pH decrease due to formation of acetic acid or gluconic acid catalyzed by esterase and GOx, respectively.<sup>[137]</sup> This part of the enzymatic process represents the OR logic gate activated by glucose (Glc) and ethyl acetate (EtOAc), Inputs A and B, respectively. The acidic pH produced enzymatically *in situ* was reset to the initial neutral pH value by producing  $\text{NH}_3$ ,

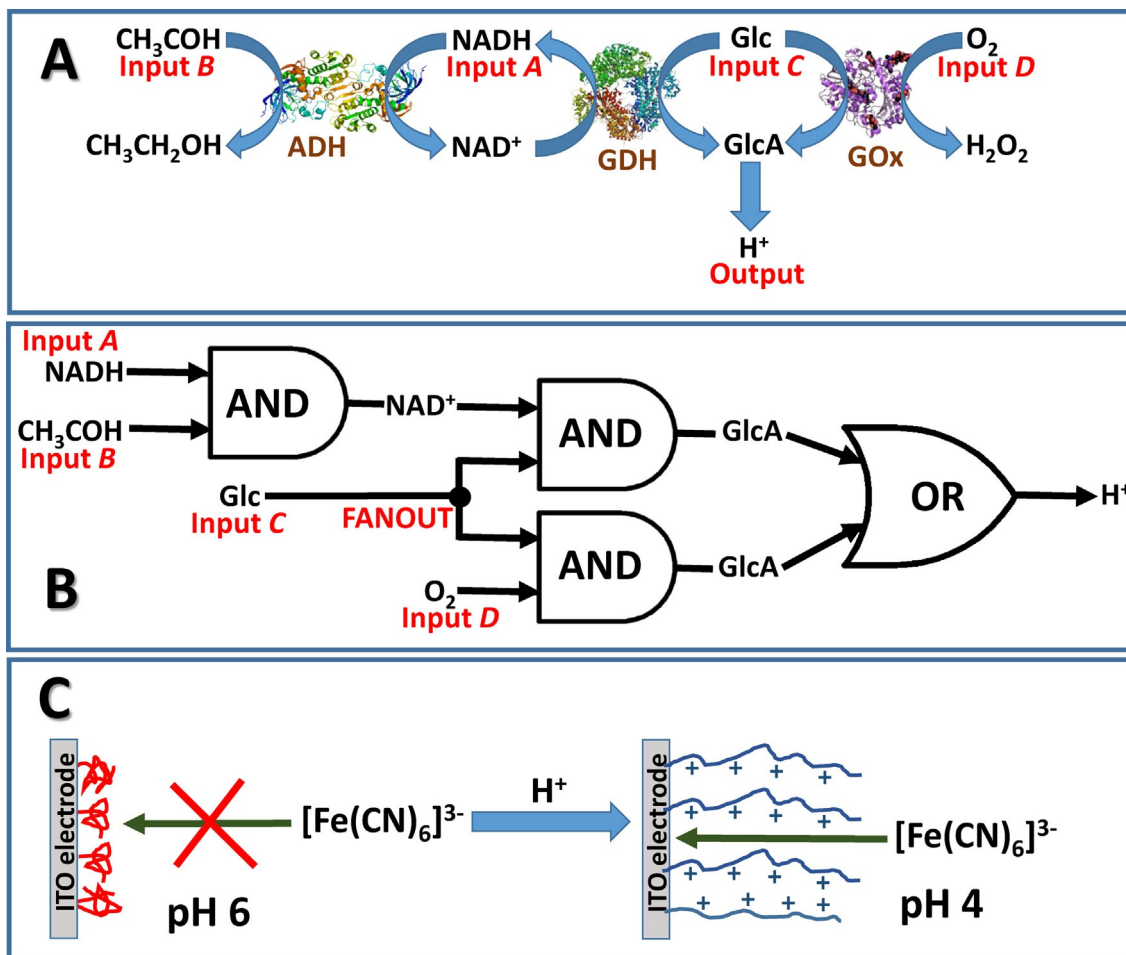


**Figure 10.** A) The biocatalytic cascade activated with four input signals and ended with oxidation of glucose to gluconic acid yielding acidic pH value. Abbreviations used in the scheme are explained in the list of abbreviations. B) The equivalent logic network corresponding to the biocatalytic cascade shown in (A). C) pH-Switchable electrode surface modified with a polymeric brush. The hydrophobic interface (left) produced at pH 6 is not permeable for the solution redox species, whereas the protonated hydrophilic interface (right) produced at pH 4 is permeable and active for the redox process of the negatively charged redox probe.

in the reaction catalyzed with urease and activated with the Reset input of urea. The pH-signal responsive system included  $\text{SiO}_2$ -NPs functionalized with a block-copolymer, PS-b-P4VP-b-PEO, composed of polystyrene (PS), poly(4-vinyl pyridine) (P4VP) and poly(ethylene oxide) (PEO) (Figure 12 B). The switchable amphiphilic  $\text{SiO}_2$ -NPs have been used as emulsifiers of Pickering emulsions.<sup>[162–166]</sup>

In Pickering emulsions, nanoparticles with amphiphilic properties, are located at the water/oil interface stabilizing different kinds of the emulsions, water-in-oil (W/O) or oil-in-water (O/W), depending on the wetting properties of the nanoparticles. The nanoparticles with more hydrophilic properties stabilize O/W emulsions, whereas nanoparticles with more hydrophobic features preferably stabilize W/O emulsions. When the wetting properties of the nanoparticles are changed upon protonation/deprotonation of their acid/base groups, the emulsion can be converted from O/W into W/O or vice versa. As an example, the nanoparticles functionalized with PS-b-P4VP-b-PEO grafted to the  $\text{SiO}_2$ -NPs surface stabilize W/O emulsions at pH ca. 6 and O/W emulsions at pH ca. 4 due to none-protonated (neu-

tral) and protonated (positively charged) states of P4VP at the corresponding pH values (Figure 13 A).

As a result, the functionalized  $\text{SiO}_2$ -NPs perform a “command” function to switch between inverse (W/O) and direct (O/W) emulsions upon receiving signals from the enzyme-catalyzed reactions. The change in the emulsion structure was read out by DC-conductivity measurements, demonstrating dramatic changes in the conductivity upon the emulsion inversion (Figure 12 C,D). After producing the O/W emulsion with a low ohmic resistance upon application of 0;1; 1;0; 1;1 input signals (note that the enzyme system was mimicking the OR gate), the emulsion was converted back into the W/O state with a high resistance by applying the Reset input bringing pH back to pH ca. 6. Figure 12 E shows the resistance measured between two electrodes immersed in the emulsion after applying different input combinations to the enzyme logic system mimicking the OR gate. Note that the final output plotted in Figure 12 E as the cell resistance ( $R_{\text{cell}}$ ) corresponds to the NOR logic gate since the resistance is decreasing when the pH is increased. Importantly, the switchable features of the  $\text{SiO}_2$ -NPs

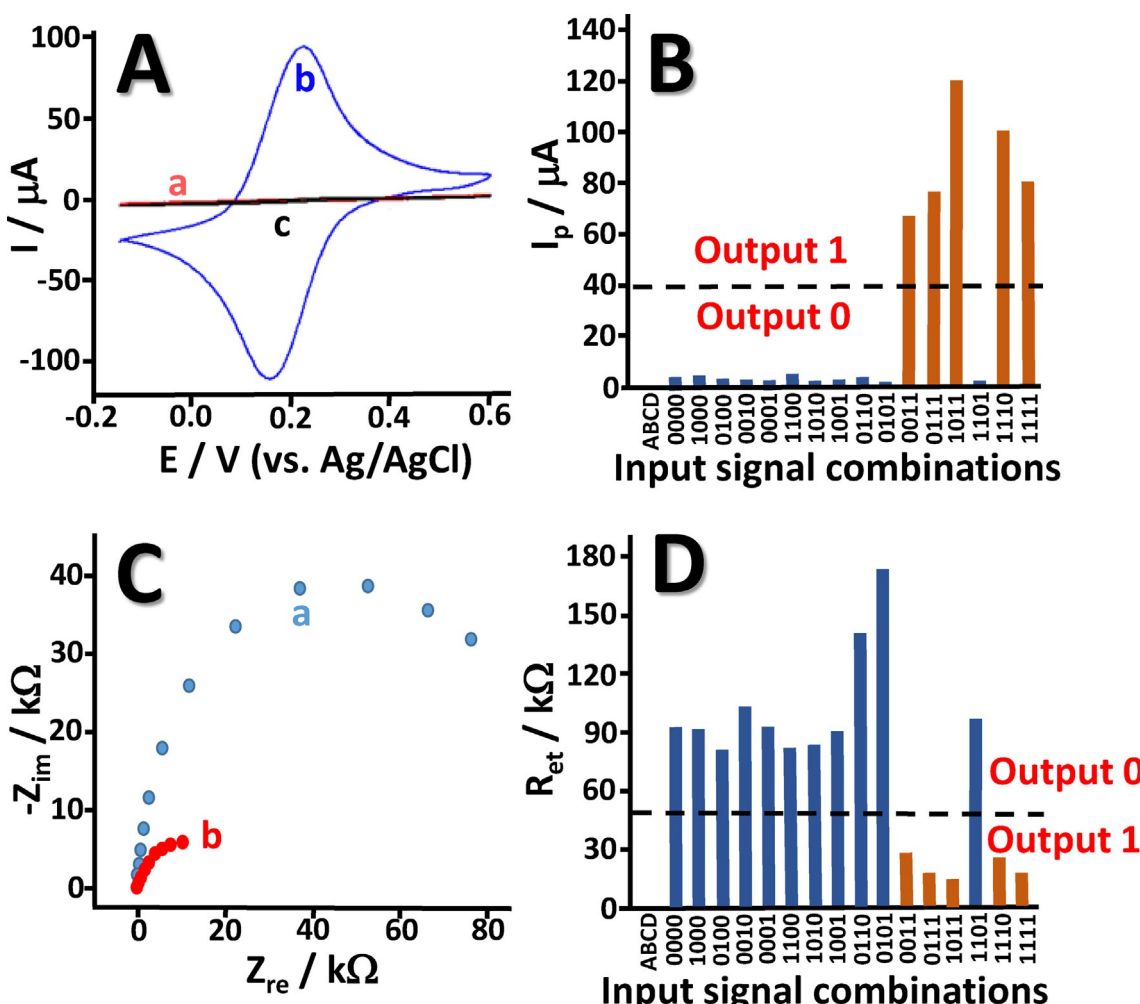


**Figure 11.** Experimental results corresponding to the system shown schematically in Figure 10. A) Cyclic voltammograms obtained for the indium tin oxide (ITO) electrode modified with the P4VP polymer brush in a) the initial OFF state, pH ca. 6.7; b) the ON state enabled by the input combination 1,1,1,0, recorded at pH ca. 4.3; and c) in situ reset to the OFF state, pH ca. 8.8. Potential scan rate was  $100 \text{ mV s}^{-1}$ . B) Anodic peak currents,  $I_p$ , for the 16 possible input combinations. The data were obtained from cyclic voltammograms recorded under the same conditions as in Panel (A). C) Faradaic impedance spectra (in the form of Nyquist plots) for a) the initial OFF state, pH ca. 6.5; b) the ON state enabled with the input combination 1,1,1,1, recorded at pH ca. 4.0. D) Electron transfer resistance,  $R_{\text{et}}$ , for the 16 possible input combinations. The data were derived from impedance spectra obtained under the same conditions as in Panel (C). The dash lines in (B) and (D) show the threshold values separating logic 1 and logic 0 output signals. Fragments of this figure were adapted from ref. [130] with permission.

interface were transduced to the changes of the bulk conductivity of the liquid system.<sup>[137]</sup> In addition to the resistance measurements, the reversible transition between the W/O and O/W emulsions was visualized by adding an oil-soluble dye coloring the oil phase (Figure 13 B,C).

#### 4.6. Transduction of Chemical Output Signals Produced by the Enzyme-Based Logic Systems Using Semiconductor Devices

Integration of the enzyme-based logic gates with field-effect devices based on an electrolyte–insulator–semiconductor (EIS) system<sup>[167–169]</sup> is the most attractive and promising approach for transduction of biomolecular logic signals into electrical output signals. Indeed, the EIS devices are electrochemical analogues of electronic elements used in conventional electronic logic gates and computing systems. Previous research, not

always related to the logic gates, has demonstrated the use of EIS devices for detection of pH changes<sup>[170]</sup> and for the analysis of enzymatic reactions<sup>[171,172]</sup> and charged macromolecules (DNA, proteins, polyelectrolytes).<sup>[173–175]</sup> Thus, the use of the EIS electronic devices is straightforward for transduction of various output signals generated by the enzyme logic systems.

It should be noted that the experimental work on the enzyme logic systems associated with the EIS devices was mostly limited to relatively simple AND, OR Boolean logic gates producing pH changes readable by the EIS device.<sup>[139–142]</sup> An example system that mimicks an OR logic gate realized by two parallel reactions catalyzed by esterase and GOx in a solution is shown schematically in Figure 14 A. Both reactions resulted in acidification of the background solution due to formation of either butyric acid or gluconic acid or both of them, if the reactions are activated by the corresponding input signals of glucose (Glc) and ethyl butyrate, Inputs A and B, respec-

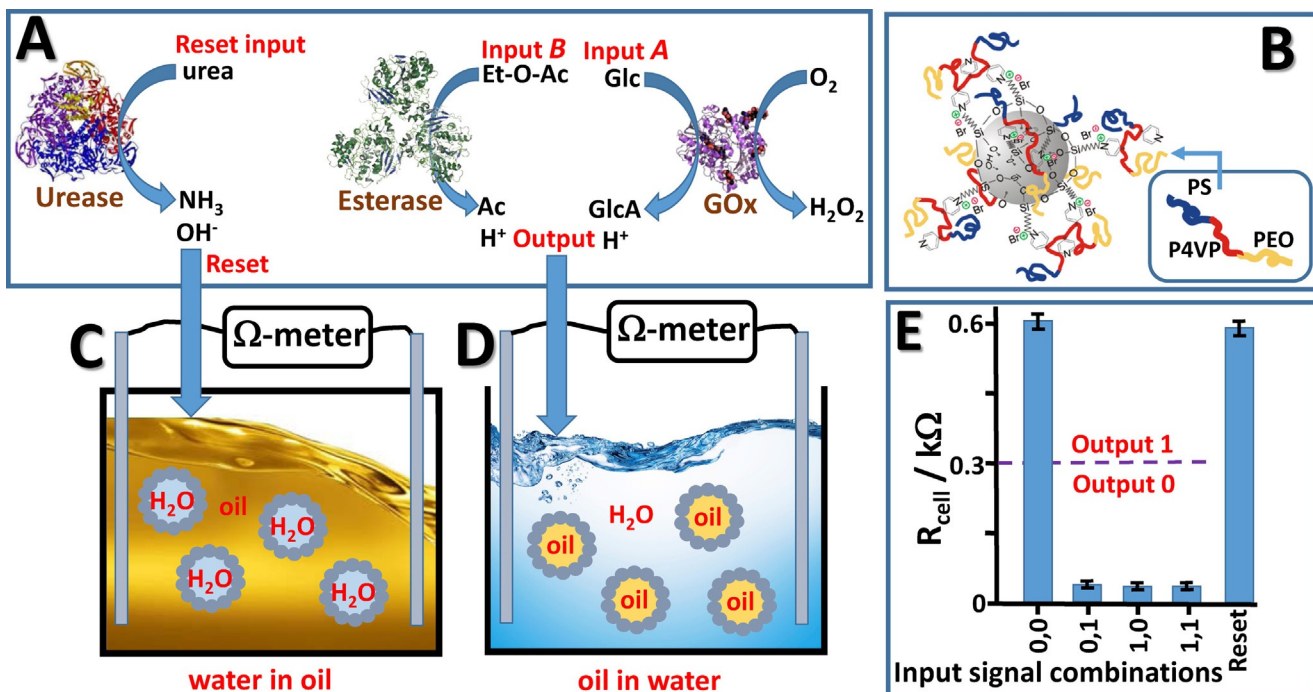


**Figure 12.** The use of DC-conductivity measurements for transducing output signals generated by the enzyme logic gate. A) The biocatalytic cascade mimicking OR gate and the biocatalytic reset system—schematics. Abbreviations used in the scheme are explained in the list of abbreviations. B) SiO<sub>2</sub>-NPs functionalized with the block-copolymer, PS-b-P4VP-b-PEO, pH-switchable brushes. C) The W/O emulsion demonstrating the high ohmic resistance for the DC-current. This emulsion was in the beginning of the experiments when the pH of the aqueous phase was ca. 6. This emulsion was also produced upon applying the Reset input. D) The O/W emulsion demonstrating the low ohmic resistance for the DC-current. This emulsion was produced when the pH of the aqueous phase was decreased to pH ca. 4 by the production of acids in the enzymatic reactions. E) A bar-chart showing the output signals in the form of the ohmic DC current resistance measured in the cell after applying the input signals in different combinations. The dash line shows the threshold value separating logic 1 and logic 0 output signals. A fragment of this figure was adapted from ref. [137] with permission.

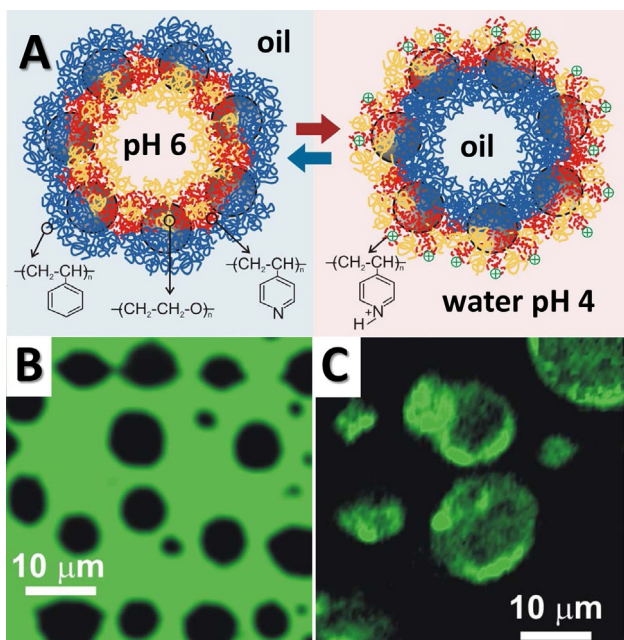


**Figure 13.** A) Water-in-oil (W/O) and oil-in-water (O/W) emulsions obtained at different pH values due to different protonation states of the pyridine units in the polymer brush bound to the SiO<sub>2</sub>-NPs. B) and C) Microscopic images of the W/O and O/W emulsions, respectively, with the oil (toluene) phase colored by adding the oil-soluble 1,4,4-tetraphenyl-1,3-butadien dye (note the green color associated with the oil phase). The figure was adapted from ref. [137] with permission.

tively.<sup>[142]</sup> Application of the input signals in three combinations: 0,1; 1,0 and 1,1 resulted in a pH decrease due to activation of either or both biocatalytic reactions. The obtained result was considered as the output signal 1. Clearly, the absence of both inputs (meaning 0,0 logic combination) did not result in any reaction and did not produce any pH change, thus generating the output signal 0. The reaction solution containing the enzymes and inputs applied in various combinations was analyzed by the pH-sensitive EIS device with the interface functionalized with Au nanoparticles coated with a thiolated monolayer containing carboxylic groups (Figure 14B). When the EIS sensing interface was exposed to the initial neutral background solution (pH 7), the carboxylic groups associated with the nanoparticles were dissociated and negatively charged. Their negative charge was preserved in case of the output signal 0 (meaning no pH change) generated by the enzyme logic system in response to 0,0 input combination. However, in the presence of the acids produced by the enzyme reactions (output signal 1) the carboxylic groups were protonated and the surface charge became neutral (Figure 14B).

Impedance spectroscopy, particularly analyzing the interfacial capacitance, was applied to follow the charge variation on the surface of the EIS device (Figure 14C). Mott-Schottky plots<sup>[176,177]</sup> derived from the impedance spectra allowed analysis of the flat band voltage ( $V_{FB}$ ) that changed as a result of the

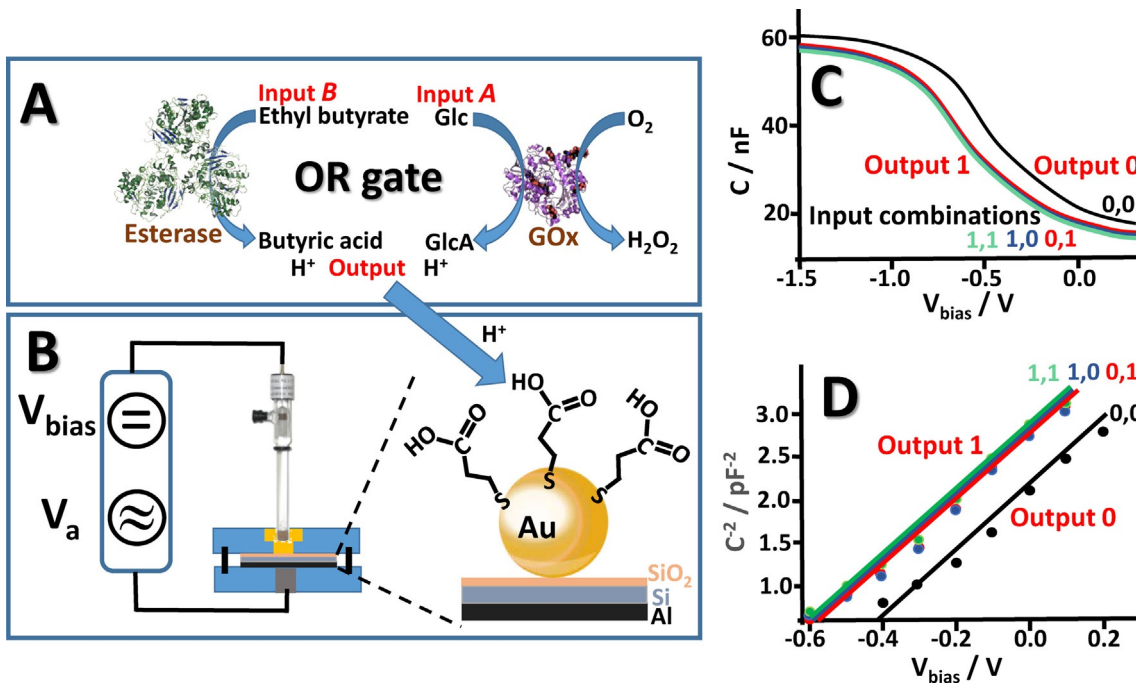


**Figure 14.** Electronic transduction of the enzyme generated output signals—the use of a semiconductor device. A) The enzyme-based OR logic gate producing pH changes as the output signal and the Reset function realized with a biocatalytic reaction. Abbreviations used in the scheme are explained in the list of abbreviations. B) Electronic scheme of the semiconductor signal-transducing device. The transducer surface is functionalized with Au NPs coated with a thiolated monolayer containing carboxylic groups. C) Capacitance vs. potential applied to the gate of the EIS device measured after application of the input signals in various combinations. D) Mott-Schottky plots derived from the impedance spectra obtained for the signal-transducing Si chip after application of the input signals in various combinations. A fragment of this figure was adapted from ref. [142] with permission.

biocatalytic reaction (Figure 14D). The interfacial capacitance and  $V_{FB}$  derived from the impedance measurements were considered as the electronic output signals converted by the EIS device from the pH variation produced by the enzyme logic gate. The changes in the EIS interfacial capacitance (Figure 14C) or shift of the Mott-Schottky function (Figure 14D) were observed when the input signals (Glc and ethyl butyrate) were applied in three different combinations (0,1; 1,0; 1,1), but not in the 0,0 combination, thus demonstrating the Boolean OR gate features. The present example is really simple in its realization, but the EIS devices can be applied to much more sophisticated logic systems. The transduction of the biochemical signals, for example pH changes, to the electronic format with the use of the semiconductor (EIS) device is conceptually important due to the demonstrated interfacing of the biomolecular logic and truly electronic systems. Full advantage of this approach can be achieved when solid-state electronics are integrated with a “soft-matter” biological logic system without soluble species involved in the signal processing steps.

## 5. Macro/Micro/Nano-Mechanical Transduction of Chemical Output Signals Produced by the Enzyme-Based Logic Systems

Enzyme-catalyzed reactions, particularly when the produced chemicals communicate with signal-responsive materials, can result in mechanical movements of objects at macro-, micro- and nano-scales.<sup>[136,161,178,179]</sup> These processes could be consid-

ered as prototypes of futuristic “smart” nano-machines and nano-robotic systems,<sup>[180,181]</sup> in which the mechanical operations are controlled by logically processed biomolecular/biological signals. In the example systems overviewed in the sections below, the mechanical transformations are considered as the final output signals produced after processing the input signal combinations through the enzyme biocatalytic cascades mimicking Boolean logic gates. Depending on the dimensions of the mechanically moving species, the technical tools used to follow the transformations range from simple photographs for macro-objects<sup>[179]</sup> to atomic force microscopy for nano-objects.<sup>[136,161]</sup>

### 5.1. Mechanical Bending of a Cantilever Used for Transduction of Chemical Output Signals Produced by the Enzyme-Based Logic Systems

Various materials, often represented by conducting electrodes, can be functionalized with conductive polymers,<sup>[182,183]</sup> particularly using polypyrrole,<sup>[184]</sup> polythiophene,<sup>[185]</sup> or polyaniline,<sup>[186]</sup> deposited on surfaces to allow control over interfacial properties that are dependent on the redox state of the polymer film. Counter ion exchange between the polymer matrices and external solutions triggered by the redox reactions in the conducting polymers results in shrinking and swelling of the polymer films, allowing their application as artificial muscles.<sup>[187]</sup> Deposition of the conducting polymers on flexible supports (e.g., polymeric strips<sup>[188–192]</sup> or micro-cantilevers)<sup>[193,194]</sup> allowed

for their mechanical bending upon reduction-oxidation of the polymer films, which is usually induced by electrochemical means. In this case, the flexible support was represented by a conducting material chemically modified with the redox polymer. Unfortunately, little attention has been given to chemically induced mechanical actuation triggered by redox transformations of the conducting polymers upon their reactions with reducing/oxidizing species applied in a solution.<sup>[179,195]</sup> The chemical, or better biochemical, activation of mechanical processes can be important for future implantable biomedical devices operating upon physiological commands, thus representing an important research direction, particularly when the mechanical operations are controlled by logically processed multiple biomolecular signals.

Figure 15 A shows a reaction cascade catalyzed by three enzymes, glucose-6-phosphate dehydrogenase (G6PDH), diaphorase (Diaph), and laccase, and activated with three signals, glucose-6-phosphate (Glc6P), NAD<sup>+</sup>, and O<sub>2</sub>, Inputs A, B and C, respectively.<sup>[179]</sup> The first enzymatic reaction catalyzed by G6PDH resulted in the production of NADH reduced species when both chemical Inputs A and B appeared, thus representing the AND logic gate. The produced NADH resulted in the formation of [Fe(CN)<sub>6</sub>]<sup>4-</sup> reduced species through the Diaph catalyzed process. On the other hand, in the presence of O<sub>2</sub> (Input C) the reaction catalyzed by laccase resulted in [Fe(CN)<sub>6</sub>]<sup>3-</sup> oxidized species. The process started in a solution containing both

[Fe(CN)<sub>6</sub>]<sup>4-</sup> and [Fe(CN)<sub>6</sub>]<sup>3-</sup> redox species. The deviation of their concentrations from the initial values to the dominated reduced or oxidized species was considered as the logic 1 output (meaning that the increase of the reduced or oxidized species is essentially the same logic output). Therefore, the process catalyzed by Diaph and laccase represents a XOR logic gate in which the unbalanced operation (input signals 0,1 and 1,0) produces output 1 and the balanced operation (input signals 0,0 and 1,1) results in the output 0. Indeed, the balanced biocatalytic reactions resulted in no changes in the [Fe(CN)<sub>6</sub>]<sup>4-</sup> and [Fe(CN)<sub>6</sub>]<sup>3-</sup> concentrations, whereas the unbalanced reactions catalyzed by either Diaph or laccase produced more [Fe(CN)<sub>6</sub>]<sup>4-</sup> or more [Fe(CN)<sub>6</sub>]<sup>3-</sup>, respectively. Figure 15B shows the equivalent logic network composed of the concatenated AND-XOR logic gates corresponding to the biocatalytic reactions. A flexible polymeric support (polyimide tape) coated with a 40-nm Au conducting film (Figure 15C) was modified with a polypyrrole (Ppy) film (ca. 8.6 μm) deposited electrochemically. When the Ppy-modified strip was in contact with the solution containing the [Fe(CN)<sub>6</sub>]<sup>4-</sup>/[Fe(CN)<sub>6</sub>]<sup>3-</sup> redox species and the enzyme logic system, the redox state of Ppy was controlled by the redox state of the species that dominated in the solution. In other words, the presence of [Fe(CN)<sub>6</sub>]<sup>4-</sup> resulted in the reduced state of Ppy, whereas [Fe(CN)<sub>6</sub>]<sup>3-</sup> yielded the oxidized state of Ppy. The Ppy-modified strip demonstrated bending upon variation of the polymer redox state,

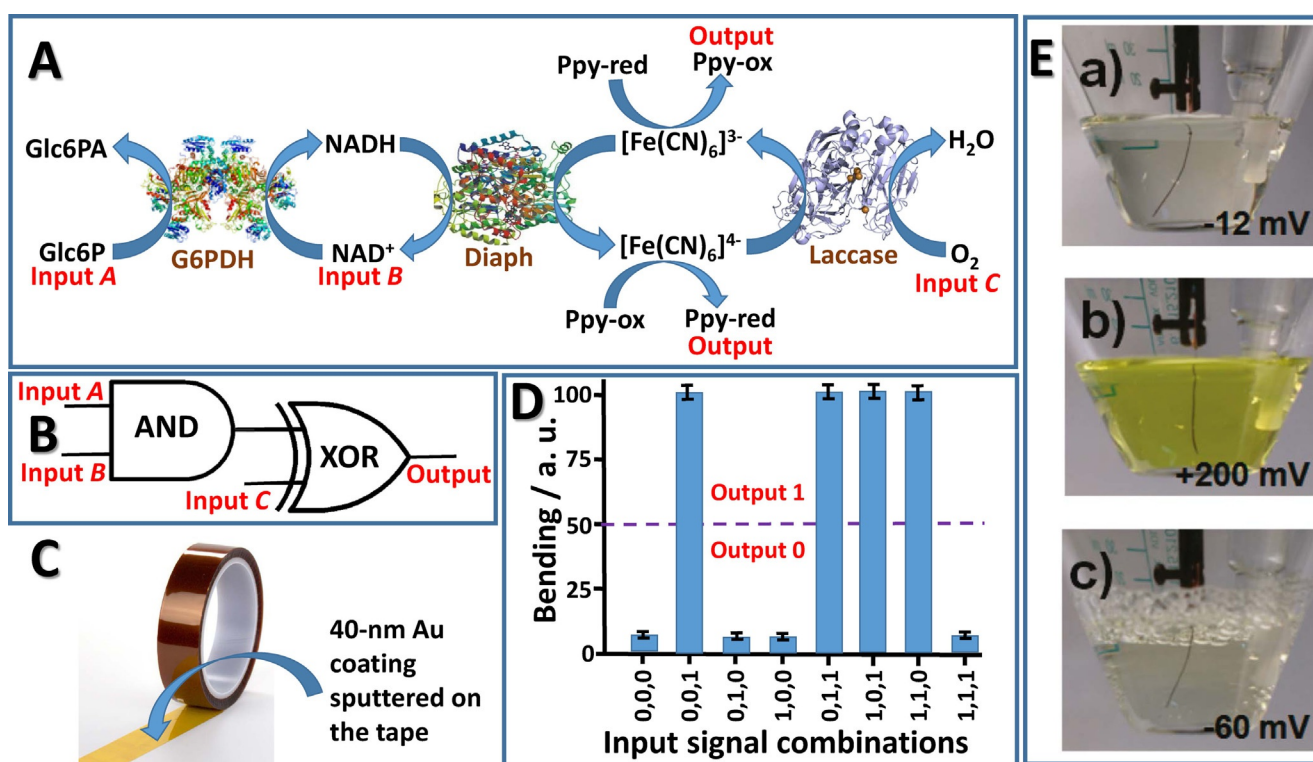


**Figure 15.** Mechanical transduction of the output signals produced by the enzyme logic gate. A) The biocatalytic cascade activated with three input signals controlling the oxidation state of [Fe(CN)<sub>6</sub>]<sup>3-</sup>/[Fe(CN)<sub>6</sub>]<sup>4-</sup> redox species. Abbreviations used in the scheme are explained in the list of abbreviations. B) The equivalent logic network corresponding to the biocatalytic cascade shown in (A). C) Flexible Au-coated tape used as a conducting support for the Ppy-film. D) The output signals in the form of tape bending after applying the input signals in different combinations. E) Images showing the bending tape when the Ppy film was in its reduced (a), oxidized (b), and again reduced (c) states. The potentials measured (vs. Ag/AgCl electrode) on the conducting tape are shown in the images. A fragment of this figure was adapted from ref. [179] with permission.

originating from the redox-induced volume changes of the polymer film, thus representing a mechanical actuator controlled by the logically processed biochemical signals. The macroscopic bending of the Ppy-strip was photographed by using a digital camera (Figure 15E). The images shown in images a–c correspond to the reduced-oxidized-reduced states of PPy and the potentials measured on the Ppy-modified strip-electrodes are given in the images. The mechanical bending of the PPy-modified strip was defined as the final output signal produced by the enzyme logic system, and it is shown in Figure 15D as the function of the input signal combinations processed by the enzymatic cascade mimicking the AND-XOR concatenated network.

## 5.2. Quartz Crystal Microbalance (QCM) Transduction of Chemical Output Signals Produced by the Enzyme-Based Logic Systems

Enzyme-catalyzed reactions can produce products that are insoluble in water and that precipitate on a solid support modified with the working enzymes. These biocatalytic reactions have been used in various biosensors, mostly based on formation of biomolecular complexes due to biorecognition processes (immune-recognition or DNA complementarity), whereas the enzymes producing the precipitating products have been used as the labels in the biomolecular complexes.<sup>[196–200]</sup> Accu-

mulation of the insoluble product on the sensing interface was analyzed by using impedance spectroscopy or quartz crystal microbalance (QCM) measurements, thus providing the bio-sensing signals. Similar biocatalytic systems mimicking logic operations and producing insoluble precipitates on solid supports can be used for microgravimetric transduction of the chemical outputs. The QCM measurements are based on change in vibration frequency of the piezoelectric device (Figure 16A) upon deposition of the insoluble material on its surface.<sup>[201]</sup>

Figure 16B shows schematically the biocatalytic cascade operated on a QCM Au-surface and mimicking an AND logic gate. Since the insoluble product should be precipitated on the QCM surface for the microgravimetric analysis, the enzymes catalyzing the reactions have to be immobilized on the sensing surface. The Au surface of the QCM sensor was modified with a self-assembled thiolated monolayer bearing active ester groups, which were used for covalent binding of horseradish peroxidase (HRP) through formation of amide bonds.<sup>[199]</sup> In the next modification step, the second enzyme, glucose oxidase (GOx), was immobilized on the HRP layer by bridging the enzymes with glutaric dialdehyde. The bi-enzyme layers biocatalytically operated in the presence of two chemical inputs, glucose (Glc) and 4-chloro-1-naphthol (CN), Inputs A and B, respectively. The glucose oxidation catalyzed by GOx resulted in the concomitant production of H<sub>2</sub>O<sub>2</sub> and the second reaction

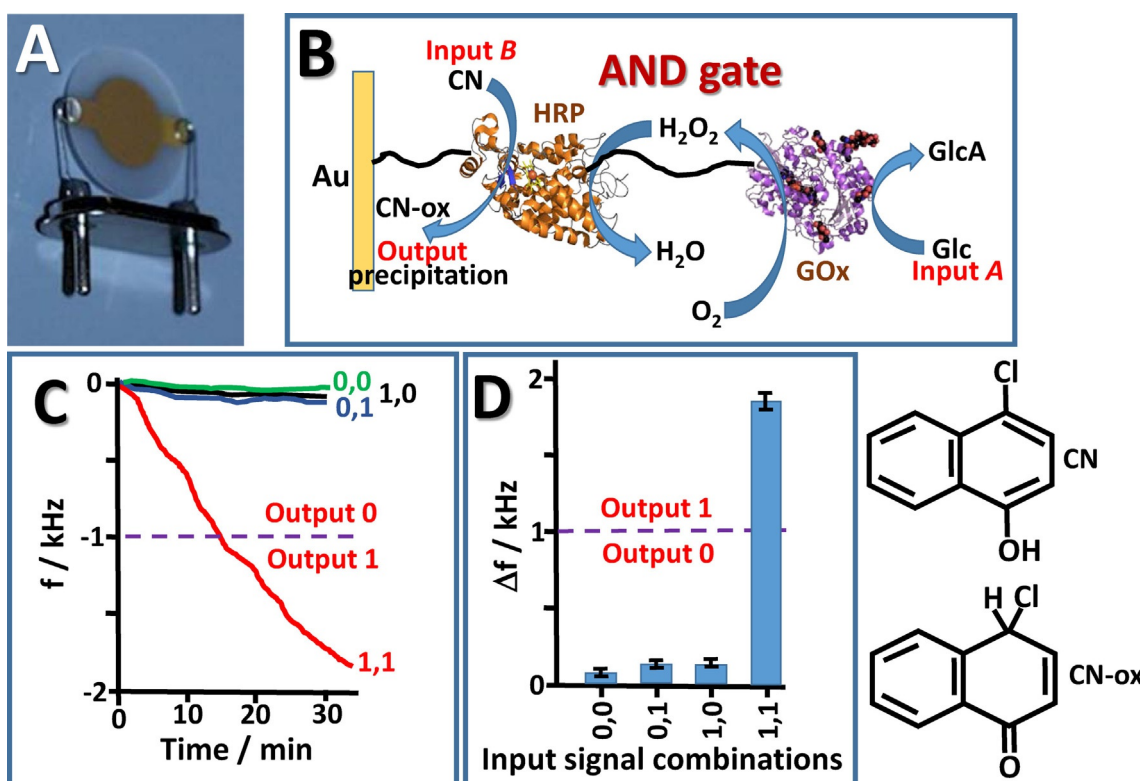


**Figure 16.** Microgravimetric transduction of the output signals produced by the enzymes logic gate. A) A QCM device used for transducing the enzyme logic gate output signals. B) The biocatalytic cascade mimicking AND gate and operating on the surface of the QCM device. The enzyme reactions result in the formation of an insoluble product precipitating on the QCM surface. Abbreviations used in the scheme are explained in the list of abbreviations. C) Frequency variation measured with the QCM device upon application of the input signals in various combinations. D) A bar-chart showing the frequency changes measured with the QCM device after 30 minutes from application of the input signals in different combinations. The structures of 4-chloro-1-naphthol (CN; Input B) and its oxidized product (CN-ox) are shown.

catalyzed by HRP resulted in oxidation of CN to insoluble oxidized product (CN-ox) precipitated on the QCM surface. The CN-ox formation was only possible in the presence of Glc and CN, in other words when Inputs A and B were applied at 1,1 combination. When one or both inputs were missing (input combinations 0,0; 0,1 and 1,0) the biocatalytic reactions did not proceed to the very end and the insoluble product was not formed on the QCM surface. Therefore, the biocatalytic cascade mimicked the AND logic gate. Figure 16C shows time-dependent frequency changes measured on the QCM when the input signals were applied in different combinations. Only 1,1 input combination resulted in a frequency change (corresponding to the output signal 1) due to deposition of the insoluble reaction product, whereas no other input combinations affected the QCM frequency (meaning output signal 0). Figure 16D summarizes the results in the form of a bar-chart showing frequency changes measured after 30 minutes from the time when the inputs were applied in different combinations. The obtained results demonstrated microgravimetric transduction of the output signals generated by the enzyme logic gate, for which the final signal was presented with the mechanical oscillation of the quartz crystal.

### 5.3. Atomic Force Microscopy (AFM) Transduction of Chemical Output Signals Produced by the Enzyme-Based Logic Systems

Nanostructured objects functionalized with signal-responsive materials can respond to the signals produced by the enzyme

logic gate. The responding nano-objects can be represented by nanoporous membranes with variable nanoporosity<sup>[136]</sup> and by nanoparticles with aggregation/disaggregation features<sup>[161]</sup> dependent on the chemical signals produced by enzymatic reactions. Nanoparticle assembly-disassembly can be triggered by chemical signals processed through biomolecular logic gates representing a biocomputing nanoplatform for therapeutics and diagnostics.<sup>[202]</sup> Biomolecular logic gates have been used to arrange dynamically gold nanoparticles on DNA origami.<sup>[203]</sup> Assembling of gold nanoparticles has been demonstrated by using a pH-responsive DNA nanomachine logically processing biomolecular input signals.<sup>[204]</sup>

Figure 17A shows the biocatalytic cascade mimicking an OR logic gate.<sup>[136]</sup> The gate “machinery” was composed of two enzymes, invertase (Inv) and glucose oxidase (GOx), and oxygen in the solution. The biocatalytic reactions were initiated by two biomolecular substrates, sucrose and glucose, Inputs A and B, respectively, applied in four different combinations. Sucrose was cut into fructose and glucose in the reaction catalyzed by Inv. Glucose produced in situ from sucrose or added as an independent input was oxidized in the reaction catalyzed by GOx yielding gluconic acid, thus decreasing the solution pH value. The acidic solution was produced in the presence of either or both inputs, sucrose or glucose, as expected for the OR logic gate. The produced acidic pH was reset to the initial neutral value by a reaction converting urea (Reset input) into NH<sub>3</sub> catalyzed by urease. Overall, the biocatalytic process represented the OR gate with the Reset function (Figure 17B). The solution with the pH controlled by the external input sig-

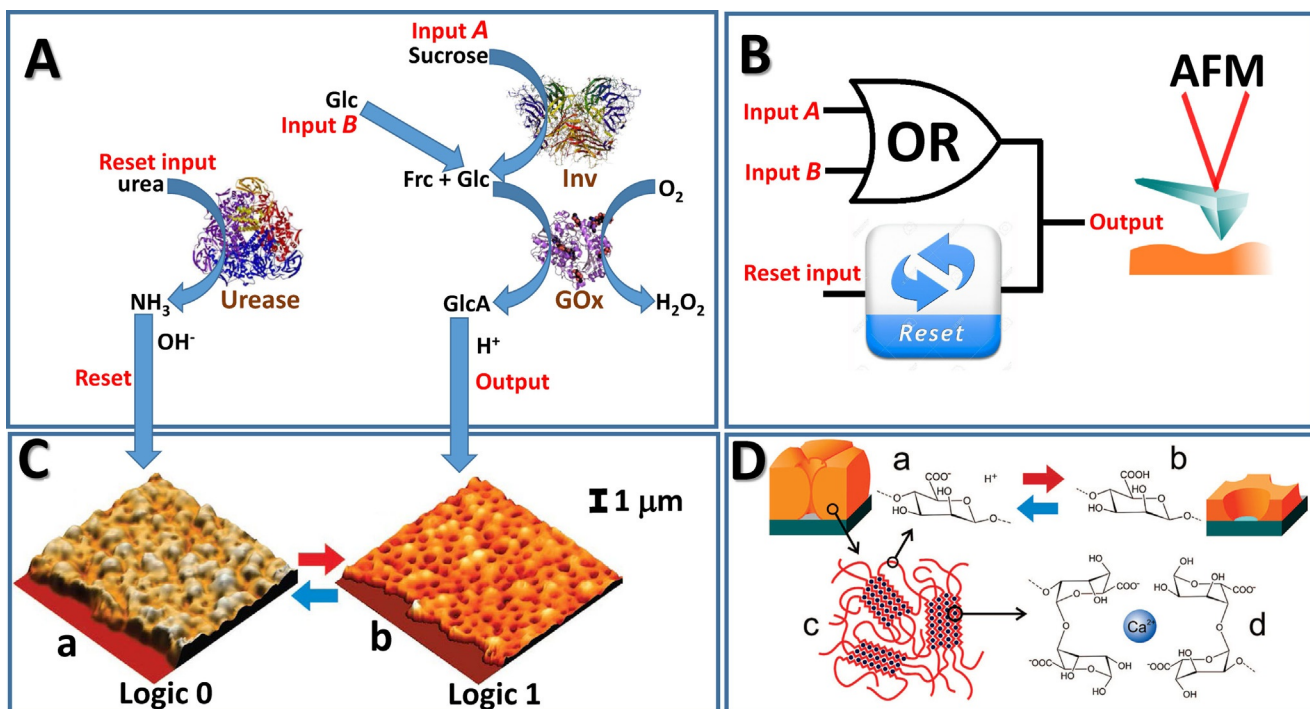


**Figure 17.** AFM transduction of the output signal produced by the enzyme logic gate—switchable porosity in a membrane. A) The biocatalytic cascade mimicking an OR logic gate and a Reset function. Abbreviations used in the scheme are explained in the list of abbreviations. B) The schematics of the OR-Reset logic device with the output transduced by AFM. C) The nanoporous membrane visualized with AFM in the closed-pore state at neutral pH (a) and open-pore state at acidic pH (b). D) Schematics showing the swollen alginate polymer resulting in the closed-pore state and shrunk polymer producing the open-pore state of the membrane. The structure of the Ca<sup>2+</sup>-cross-linked alginate is shown. A fragment of this figure was adapted from ref. [136] with permission.

nals was in immediate contact with a pH-switchable nanoporous membrane (Figure 17C) composed of alginate hydrogel<sup>[205]</sup> comprised of D-mannuronic acid and L-guluronic acid residues cross-linked with Ca<sup>2+</sup> cations (Figure 17D). At the initial neutral pH, the alginate polymer contains deprotonated (negatively charged) carboxylic groups, thus being hydrophilic and swollen. The swollen polymer matrix expands in volume and closes completely the nanopores in the membrane body. When the solution pH is decreased below the pK<sub>a</sub> of the alginate polymer (pH < 4), the carboxylic groups become protonated, resulting in their neutral charge, thus yielding the hydrophobic shrunk polymer. This results in opening of the nanopores (380 ± 116 nm measured by AFM at the half-depth of the pores). The reset of the solution pH to the initial neutral value returns the nanopores to their closed state (Figure 17C). The operation of the enzyme logic system was based on the pH variation due to the biocatalytic reactions. Clearly, the pH variation can be measured directly with a pH-sensitive electrode or indirectly by following the membrane permeability controlled by the pH value. The latter was measured by observing molecular diffusion through the pores and by measuring the membrane impedance when the membrane was deposited on an electrode surface. However, for the present section of the

review, it is important to emphasize that the membrane state was analyzed with atomic force microscopy (AFM) (Figure 17C). The membrane state with the open nanopores (output signal 1) was achieved when the input signals were applied at 0,1; 1,0 and 1,1 combinations, otherwise the closed pore state (output signal 0) was obtained with the input combination 0,0 (Figure 17C). The membrane was reset to the initial state by the Reset signal after the output signal 1 was produced.

A similar biocatalytic cascade (Figure 18A), but using enzymes as the input signals (Inv and GOx, Inputs A and B, respectively), was used to variate the solution pH and then control aggregation and dissociation of SiO<sub>2</sub>-NPs (200 nm) functionalized with poly(2-vinyl pyridine) (P2VP) polyelectrolyte.<sup>[161]</sup> Despite the fact that the biocatalytic cascade was the same as in the previous example, the new definition of the input signals resulted in a different logic function. Indeed, the final output signal (GlcA producing acidic pH value) was obtained only when both biocatalytic reactions proceeded in the presence of both input signals (both enzymes present). At the initial neutral pH value the P2VP-polymer was deprotonated and neutral. This resulted in aggregation of the neutral NPs, thus yielding their aggregates with a large size. When the pH value

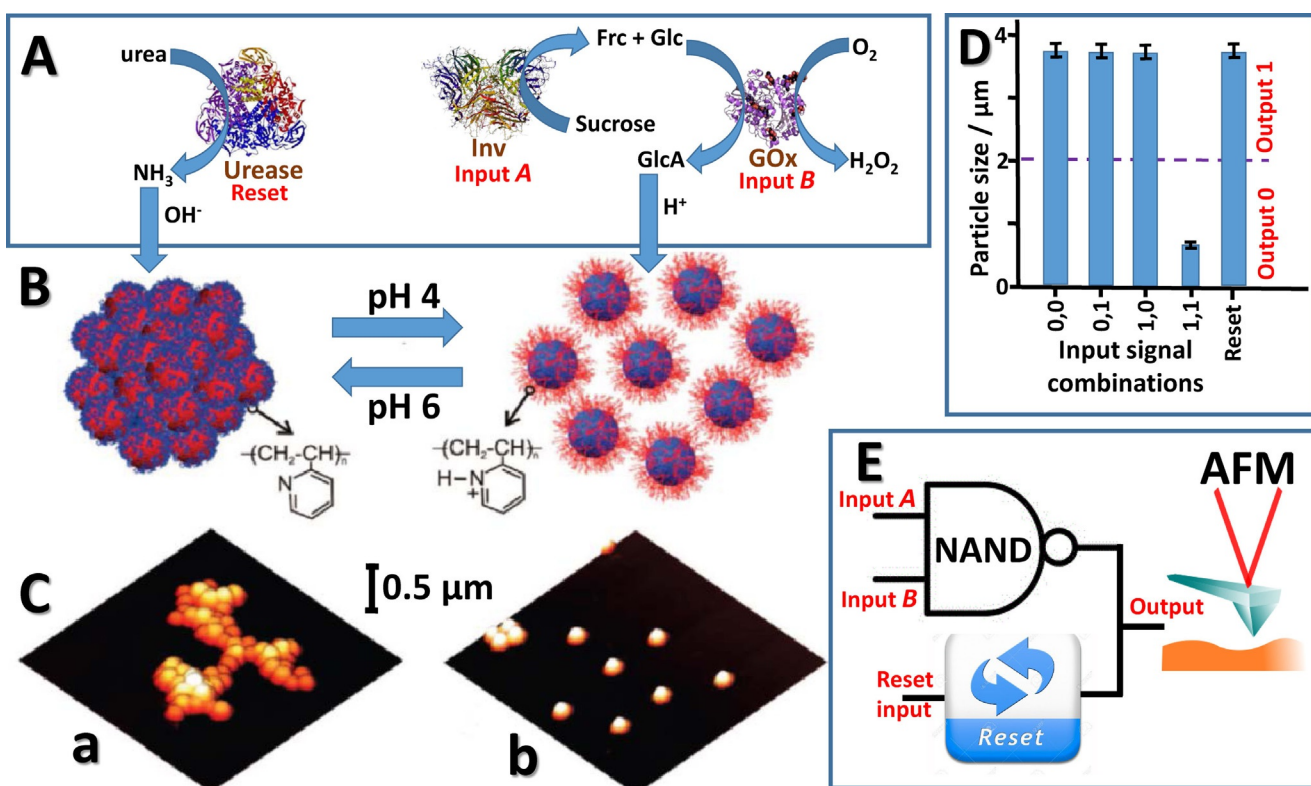


**Figure 18.** AFM transduction of the output signal produced by the enzyme logic gate—switchable aggregation/disaggregation of nanoparticles (NPs). A) The biocatalytic cascade mimicking an NAND logic gate and a Reset function. Abbreviations used in the scheme are explained in the list of abbreviations. B) Reversible aggregation/disaggregation of the NPs controlled by pH values. The NPs were functionalized with P2VP polymer brushes changing their charge at different pH values due to the pyridine group protonation (pH 4) and deprotonation (pH 6). C) AFM images of the aggregated (a) and disaggregated (b) nanoparticles after their deposition on a surface. D) A bar-chart showing the size of the NPs in their aggregated and disaggregated states obtained upon application of the input signals in different combinations and after applying the reset signal. The dash line shows the threshold value separating logic 1 and logic 0 output signals. E) Schematics of the NAND-Reset logic device with the output transduced by AFM. A fragment of this figure was adapted from ref. [161] with permission.

was decreased ( $\text{pH} < 4$ ) due to acidification of the solution with the *in situ* produced GlcA, the pyridine units of P2VP-polymer were protonated, bringing a positive charge to the NPs. The positively charged NPs were dissociated from their aggregates, revealing their small size (Figure 18B). The size of the nanospecies in their aggregated and dissociated states was measured *ex situ*, observing the structures deposited from the suspensions on Si wafers with AFM (Figure 18C). The large size aggregates were defined as the output signal 1, whereas the small size disaggregated NPs were considered as the output signal 0. The output 0 was obtained only when both enzyme inputs were present to complete the biocatalytic cascade (input signal combination 1,1), whereas all other input combinations (0,0; 0,1; 1,0) resulted in no formation of acidic pH, thus keeping the NPs in their aggregated state (meaning the output signal 1). This logic operation corresponds to the NAND gate (Figure 18D). The reset to the initial neutral pH, returning the dissociated NPs to the aggregated state, was achieved with the biocatalytic reaction producing  $\text{NH}_3$  (Figure 18A). Overall, the studied system resembles the NAND-Reset function, which was followed by AFM measurements (Figure 18E).

The systems exemplified above are also interesting because they demonstrated the nanomechanical actuation logically controlled by the pH signals produced *in situ* through biocatalytic reactions. Furthermore, it should be noted that simple reformulation of the input signal definitions can result in different logic operations (OR/NAND in the given examples).

## 6. Conclusions and Perspectives

The majority of research papers, review articles and books overviewing progress in biomolecular<sup>[18–23]</sup> (including enzyme-based)<sup>[24,25]</sup> and molecular<sup>[6–17]</sup> logic gates concentrate on their composition and performance, while giving little attention to the methods of the output signal transduction. The present review aims to highlight the underrepresented aspects of biomolecular computing, specifically collecting examples of the enzyme logic systems connected to different physical methods of the output signal transduction. Whereas the most frequently used method is based on optical absorbance measurements after performing biocatalytic reactions in solutions, other methods, especially those based on electrochemical techniques, are highly important. Electrochemical interfaces, particularly those functionalized with signal-responsive materials, operating with the enzyme-based logic systems demonstrated significant advantages over the optical readout of the chemical output signals. It should be noted that the optical tools applied to the analysis of the output signals allow only the signal readout, whereas electrochemical interfaces can operate as actuators triggered by the biomolecular computing systems. Indeed, electrochemical systems can release molecular/biomolecular species in response to the signals processed by the enzyme logic gates, thus activating downstream reactions and processes,<sup>[126,127]</sup> for example releasing DNA species, activating next logic steps in the DNA computing process. The electrochemical signal-transduces can also switch ON/OFF various

bioelectrochemical devices (e.g., biofuel cells)<sup>[44]</sup> in response to the logically processed biomolecular signals.

Electrochemical interfaces<sup>[80]</sup> releasing DNA species (short artificial oligonucleotides) in response to the output signals generated by the enzyme logic systems resulted in the unique integration of enzyme-based and DNA-based logic elements in highly sophisticated hybrid computing systems,<sup>[126,127]</sup> benefiting from the features of the enzyme and DNA components. These systems allow logically reversible processing of the initial input signals through the enzyme and DNA reactions, and they are particularly beneficial for biosensing applications when the restoration of the initial signal pattern from the final output signals is important.

Simple single-output producing logic gates (e.g., AND, OR, NAND, XOR, etc.) can easily operate as a “one-pot” system, being assembled in a solution or on a transducer surface. However, when more sophisticated logic systems composed of concatenated/branched logic elements and producing several output signals are required, the use of a “one-pot” structure becomes difficult because of cross-talking of the logic elements and overlapping of the output signals. This makes the readout of the output signals particularly difficult when optical absorbance is used as the signal transduction method. One of the approaches used to solve the problem and to allow the increasing complexity of the logic systems is the spatial separation of the logic elements and organizing the output signals through physically different channels; for example, in multi-channel flow devices.<sup>[40,56,57,65,98]</sup> Application of different transduction methods to follow the output signals is highly important for increasing complexity of the biomolecular logic systems, particularly when the system generates several signals that are measured separately. An example system comprised of several concatenated logic gates based on a biocatalytic reaction cascade was used to illustrate the advantages of reading the output signals through different transduction mechanisms, including optical absorbance measurements and bioluminescence.<sup>[60]</sup> Application of AFM for reading output signals generated by biomolecular logic systems allows extremely high sensitivity, up to detection of single molecules, because the detection process can be localized on a very small surface area.<sup>[206–208]</sup>

Although the present review article is concentrated specifically on the read-out methods for the output signals generated by the enzyme logic systems, other biomolecular computing assemblies, particularly including DNA-based logic systems,<sup>[22,23,29,209–212]</sup> can be combined with various detection methods discussed in the article. Particularly, catalytic reactions activated by DNAzymes in the presence of various combinations of inputs can be analyzed by the methods developed for the analysis of the biocatalytic logic systems based on the enzyme reactions.<sup>[126,127]</sup> Indeed, many other transducing methods can be envisaged for various biomolecular logic systems, including, for example, electroluminescence as the signal detection tool.<sup>[213]</sup>

Overall, the biomolecular computing systems, and particularly enzyme-based logic gates and networks, can contribute not only to the design of future “biocomputers”, which are not

possible at the present level of technology, but on a short term to the development of novel binary-operating biosensors with various transduction tools of the logically processed bio-signals. It should be noted that the biomolecular information processing systems demonstrated promising results while operating in a biological environment<sup>[36]</sup> dealing with real biological samples,<sup>[214–216]</sup> thus giving rise to the expectations of their real practical applications, particularly in therapeutics and diagnostics,<sup>[202]</sup> and in forensic investigations.<sup>[216]</sup>

## Abbreviations:

$\alpha$ -KTG	$\alpha$ -ketoglutaric acid	LSPR	localized surface plasmon resonance
Abs	optical absorbance	Luc	luciferase (enzyme from ATP assay kit, Sigma-Aldrich)
ABTS	2,2'-azino-bis(3-ethylbenzothiazoline-6-sulfonic acid) (chromogenic substrate used to follow peroxidase activity)	Lucif	luciferin
ABTS <sub>ox</sub>	oxidized ABTS (colored product)	MPh	maltose phosphorylase (enzyme; EC 2.4.1.8)
Ac	acetic acid	NAD <sup>+</sup>	nicotinamide adenine dinucleotide
ADH	alcohol dehydrogenase (enzyme; EC 1.1.1.1)	NADH	nicotinamide adenine dinucleotide reduced
ADP	adenosine 5'-diphosphate	NPs	nanoparticles
AFM	atomic force microscope (microscopy)	O/W	oil-in-water Pickering emulsion
Ala	alanine (amino acid)	P2VP	poly(2-vinyl pyridine)
Ald	acetaldehyde	P4VP	poly(4-vinyl pyridine)
ALT	alanine transaminase (enzyme; EC 2.6.1.2)	PB	Prussian Blue
AGS	amyloglucosidase (enzyme; EC 3.2.1.3)	PEO	poly(ethylene oxide)
ATP	adenosine 5'-triphosphate	PEP	phospho(enol)pyruvic acid (or phosphoenol pyruvate in the form of salt)
CN	4-chloro-1-naphthol	Pi	inorganic phosphate
CN-ox	CN insoluble oxidized product	PK	pyruvate kinase (enzyme; EC 2.7.1.40)
DC	direct current	Ppy	polypyrrole
Diaph	diaphorase (enzyme; EC 1.8.1.4)	Ppy-ox	polypyrrole oxidized state
DNA	deoxyribonucleic acid	Ppy-red	polypyrrole reduced state
EIS	electrolyte-insulator-semiconductor	PQQ	pyrroloquinoline quinone
Et-O-Ac	ethyl acetate	PS	polystyrene
EtOH	ethanol	Pyr	pyruvate
FET	field-effect transistor	QCM	quartz crystal microbalance
Frc	fructose	R	reflectance measured by SPR
G6PDH	glucose 6-phosphate dehydrogenase (enzyme; EC 1.1.1.49)	R <sub>cell</sub>	ohmic resistance measured in a bulk solution in an electrochemical cell
GDH	glucose dehydrogenase (enzyme; EC 1.1.1.47)	R <sub>et</sub>	electron transfer resistance (measured by Faradaic impedance spectroscopy)
Glc	glucose	RE	reference electrode
Glc6P	glucose-6-phosphate	RNA	ribonucleic acid
Glc6PA	gluconate-6-phosphate acid (product of Glc6P oxidation)	SPR	surface plasmon resonance
GlcA	gluconic acid	TBI	traumatic brain injury
Glu	glutamate (amino acid, salt form)	TMB	3,3',5,5'-tetramethylbenzidine (chromogenic substrate used to follow peroxidase activity)
GluOx	glutamate oxidase (enzyme; EC 1.4.3.11)	UV	ultraviolet
GOx	glucose oxidase (enzyme; EC 1.1.3.4)	V <sub>a</sub>	alternative voltage applied between the conducting support and reference electrode of the EIS devise
HK	hexokinase (enzyme; EC 2.7.1.1)	V <sub>bias</sub>	constant (bias) voltage applied between the conducting support and reference electrode of the EIS devise
HRP	horseradish peroxidase (enzyme; EC 1.11.1.7)	V <sub>FB</sub>	flat band voltage of the EIS device
Inv	invertase (enzyme; EC 3.2.1.26)	W/O	water-in-oil Pickering emulsion
I <sub>p</sub>	peak current (measured with cyclic voltammetry)		
IR	infrared		
ITO	indium tin oxide (electrode)		
Lac	lactate		
LDH	lactate dehydrogenase (enzyme; EC 1.1.1.27)		

## Acknowledgements

This work was supported by National Science Foundation (award CBET-1403208).

## Conflict of interest

The author declares no conflict of interest.

**Keywords:** analytical methods • biocomputing • enzymes • logic gates • transduction methods

- [1] *Unconventional Computation. Lecture Notes in Computer Science*, Vol. 5715 (Eds.: C. S. Calude, J. F. Costa, N. Dershowitz, E. Freire, G. Rozenberg), Springer, Berlin, 2009.
- [2] M. Freebody, *Photonics Spectra* 2011, 45, 45–47.
- [3] J. R. Powell, *Proc. IEEE* 2008, 96, 1247–1248.
- [4] C. Brown, G. Linden, *Chips and Change: How Crisis Reshapes the Semiconductor Industry*, MIT, Cambridge, 2009, Chap. 5, pp. 95–106.
- [5] K. Rupp, S. Selberherr, *IEEE Trans. Semiconductor Manufacturing* 2011, 24, 1–4.
- [6] K. Szacilowski, *Infochemistry—Information Processing at the Nanoscale*, Wiley, Chichester, 2012.
- [7] A. P. de Silva, *Molecular Logic-Based Computation*, Royal Society of Chemistry, Cambridge, 2013.
- [8] *Molecular and Supramolecular Information Processing—From Molecular Switches to Unconventional Computing* (Ed.: E. Katz), Wiley-VCH, Weinheim, 2012.
- [9] *Molecular Computing* (Eds.: T. Sienko, A. Adamatzky, M. Conrad, N. G. Rambidi), MIT, Cambridge, 2003.
- [10] A. P. de Silva, *Nature* 2008, 454, 417–418.
- [11] A. P. de Silva, *Nat. Nanotechnol.* 2007, 2, 399–410.
- [12] A. P. de Silva, S. Uchiyama, T. P. Vance, B. Wannalserse, *Coord. Chem. Rev.* 2007, 251, 1623–1632.
- [13] A. Credi, *Angew. Chem. Int. Ed.* 2007, 46, 5472–5475; *Angew. Chem.* 2007, 119, 5568–5572.
- [14] U. Pischel, J. Andreasson, D. Gust, V. F. Pais, *ChemPhysChem* 2013, 14, 28–46.
- [15] U. Pischel, *Angew. Chem. Int. Ed.* 2010, 49, 1356–1358; *Angew. Chem.* 2010, 122, 1396–1398.
- [16] K. Szacilowski, *Chem. Rev.* 2008, 108, 3481–3548.
- [17] J. Andréasson, U. Pischel, *Chem. Soc. Rev.* 2015, 44, 1053–1069.
- [18] *Biomolecular Computing—From Logic Systems to Smart Sensors and Actuators* (Ed.: E. Katz), Wiley-VCH, Weinheim, 2012.
- [19] D. Q. Fan, J. B. Zhu, Y. Q. Liu, E. K. Wang, S. J. Dong, *Nanoscale* 2016, 8, 3834–3840.
- [20] Y. Benenson, *Nat. Rev. Genet.* 2012, 13, 455–468.
- [21] L. Qian, E. Winfree, *J. R. Soc. Interface* 2011, 8, 1281–1297.
- [22] M. N. Stojanovic, D. Stefanovic, S. Rudchenko, *Acc. Chem. Res.* 2014, 47, 1845–1852.
- [23] M. N. Stojanovic, D. Stefanovic, *J. Comput. Theor. Nanosci.* 2011, 8, 434–440.
- [24] E. Katz, V. Privman, *Chem. Soc. Rev.* 2010, 39, 1835–1857.
- [25] E. Katz, *Curr. Opin. Biotechnol.* 2015, 34, 202–208.
- [26] Y. Benenson, *Mol. BioSyst.* 2009, 5, 675–685.
- [27] A. R. Pease, J. F. Stoddart in *Molecular Machines and Motors, Book Series: Structure and Bonding*, Vol. 99 (Ed.: J.-P. Sauvage), Springer, Berlin, 2001, pp. 189–236.
- [28] J. C. Claussen, N. Hildebrandt, K. Susumu, M. G. Ancona, I. L. Medintz, *ACS Appl. Mater. Interfaces* 2014, 6, 3771–3778.
- [29] Z. Ezziane, *Nanotechnology* 2006, 17, R27–R39.
- [30] Z. Xie, L. Wroblewska, L. Prochazka, R. Weiss, Y. Benenson, *Science* 2011, 333, 1307–1311.
- [31] G. Ashkenasy, Z. Dadon, S. Alesebi, N. Wagner, N. Ashkenasy, *Isr. J. Chem.* 2011, 51, 106–117.
- [32] R. Unger, J. Moult, *Proteins* 2006, 63, 53–64.
- [33] K. Rinaudo, L. Bléri, R. Maddamsetti, S. Subramanian, R. Weiss, Y. Benenson, *Nat. Biotechnol.* 2007, 25, 795–801.
- [34] M. A. Arugula, N. Shroff, E. Katz, Z. He, *Chem. Commun.* 2012, 48, 10174–10176.
- [35] A. Adamatzky, *Physarum Machines: Computers from Slime Mould*, World Scientific, Singapore, 2010.
- [36] M. Kahan, B. Gil, R. Adar, E. Shapiro, *Phys. D* 2008, 237, 1165–1172.
- [37] M. N. Stojanovic, D. Stefanovic, *J. Am. Chem. Soc.* 2003, 125, 6673–6676.
- [38] Y. Benenson, *Nat. Nanotechnol.* 2011, 6, 465–467.
- [39] R. Baron, O. Lioubashevski, E. Katz, T. Niazov, I. Willner, *Angew. Chem. Int. Ed.* 2006, 45, 1572–1576; *Angew. Chem.* 2006, 118, 1602–1606.
- [40] B. E. Fratto, J. M. Lewer, E. Katz, *ChemPhysChem* 2016, 17, 2210–2217.
- [41] H. L. Li, S. J. Guo, Q. H. Liu, L. D. Qin, S. J. Dong, Y. Q. Liu, E. K. Wang, *Adv. Sci.* 2015, 2, 1500054.
- [42] M. Pita, S. Minko, E. Katz, *J. Mater. Sci.: Mater. Med.* 2009, 20, 457–462.
- [43] M. Zhou, Y. Du, C. G. Chen, B. L. Li, D. Wen, S. J. Dong, E. K. Wang, *J. Am. Chem. Soc.* 2010, 132, 2172–2174.
- [44] E. Katz, M. Pita, *Chem. Eur. J.* 2009, 15, 12554–12564.
- [45] G. Strack, M. Ornatska, M. Pita, E. Katz, *J. Am. Chem. Soc.* 2008, 130, 4234–4235.
- [46] J. H. Chen, S. G. Zhou, J. L. Wen, *Angew. Chem. Int. Ed.* 2015, 54, 446–450; *Angew. Chem.* 2015, 127, 456–460.
- [47] J. Wang, E. Katz, *Isr. J. Chem.* 2011, 51, 141–150.
- [48] J. Wang, E. Katz, *Anal. Bioanal. Chem.* 2010, 398, 1591–1603.
- [49] A. Prokup, J. Hemphill, A. Deiters, *J. Am. Chem. Soc.* 2012, 134, 3810–3815.
- [50] Y. V. Gerasimova, D. M. Kolpashchikov, *Chem. Asian J.* 2012, 7, 534–540.
- [51] Y. H. Guo, L. Zhou, L. J. Xu, X. D. Zhou, J. M. Hu, R. J. Pei, *Sci. Rep.* 2014, 4, 7315.
- [52] S. Roy, M. Prasad, *Opt. Eng.* 2010, 49, 065201.
- [53] J. P. Klein, T. H. Leete, H. Rubin, *Biosystems* 1999, 52, 15–23.
- [54] C. Zhou, K. Wang, D. Fan, C. Wu, D. Liu, Y. Liu, E. Wang, *Chem. Commun.* 2015, 51, 10284–10286.
- [55] F. Moseley, J. Halámek, F. Kramer, A. Poghossian, M. J. Schöning, E. Katz, *Analyst* 2014, 139, 1839–1842.
- [56] B. E. Fratto, E. Katz, *ChemPhysChem* 2015, 16, 1405–1415.
- [57] B. E. Fratto, E. Katz, *ChemPhysChem* 2016, 17, 1046–1053.
- [58] T. Niazov, R. Baron, E. Katz, O. Lioubashevski, I. Willner, *Proc. Natl. Acad. Sci. USA* 2006, 103, 17160–17163.
- [59] V. Privman, M. A. Arugula, J. Halámek, M. Pita, E. Katz, *J. Phys. Chem. B* 2009, 113, 5301–5310.
- [60] N. Guz, J. Halámek, J. F. Rusling, E. Katz, *Anal. Bioanal. Chem.* 2014, 406, 3365–3370.
- [61] S. Bi, M. Chen, X. Q. Jia, Y. Dong, Z. H. Wang, *Angew. Chem. Int. Ed.* 2015, 54, 8144–8148; *Angew. Chem.* 2015, 127, 8262–8266.
- [62] M. N. Stojanovic, D. Stefanovic, *Nat. Biotechnol.* 2003, 21, 1069–1074.
- [63] W. Sun, C. H. Xu, Z. Zhu, C. J. Fang, C. H. Yan, *J. Phys. Chem. C* 2008, 112, 16973–16983.
- [64] M. Pita, E. Katz, *J. Am. Chem. Soc.* 2008, 130, 36–37.
- [65] B. E. Fratto, L. J. Roby, N. Guz, E. Katz, *Chem. Commun.* 2014, 50, 12043–12046.
- [66] S. Q. Zhang, K. Wang, C. C. Huang, T. Sun, *Nanoscale* 2015, 7, 20749–20756.
- [67] P. Ball, *Nature* 2000, 406, 118–120.
- [68] E. Katz, V. Bocharova, M. Privman, *J. Mater. Chem.* 2012, 22, 8171–8178.
- [69] S. Minko, E. Katz, M. Motornov, I. Tokarev, M. Pita, *J. Comput. Theor. Nanosci.* 2011, 8, 356–364.
- [70] X. Yu, W. J. Lian, J. N. Zhang, H. Y. Liu, *Biosens. Bioelectron.* 2016, 80, 631–639.
- [71] E. Gdor, S. Shemesh, S. Magdassi, D. Mandler, *ACS Appl. Mater. Interfaces* 2015, 7, 17985–17992.
- [72] O. B. Ayyub, P. Kofinas, *ACS Nano* 2015, 9, 8004–8011.
- [73] Y. Y. Huang, X. Ran, Y. H. Lin, J. S. Ren, X. G. Qu, *Anal. Chim. Acta* 2015, 870, 92–98.
- [74] L. Wang, W. J. Lian, H. Q. Yao, H. Y. Liu, *ACS Appl. Mater. Interfaces* 2015, 7, 5168–5176.
- [75] L. Ma, A. P. Diao, *Chem. Commun.* 2015, 51, 10233–10235.
- [76] T. Miyake, E. E. Josberger, S. Keene, Y. X. Deng, M. Rolandi, *APL Mater.* 2015, 3, 014906.
- [77] S. Liu, L. Wang, W. J. Lian, H. Y. Liu, C. Z. Li, *Chem. Asian J.* 2015, 10, 225–230.
- [78] M. Ikeda, T. Tanida, T. Yoshii, K. Kurotani, S. Onogi, K. Urayama, I. Hamachi, *Nat. Chem.* 2014, 6, 511–518.
- [79] J. Guo, J. M. Zhuang, F. Wang, K. R. Raghupathi, S. Thayumanavan, *J. Am. Chem. Soc.* 2014, 136, 2220–2223.
- [80] Y. M. Jia, R. X. Duan, F. Hong, B. Y. Wang, N. N. Liu, F. Xia, *Soft Matter* 2013, 9, 6571–6577.
- [81] J. H. Chen, L. W. Zeng, *Biosens. Bioelectron.* 2013, 42, 93–99.
- [82] W. T. Liu, L. Y. Wu, S. Y. Yan, R. Huang, X. C. Weng, X. Zhou, *Anal. Methods* 2013, 5, 3631–3634.
- [83] K. Radhakrishnan, J. Tripathy, A. M. Raichur, *Chem. Commun.* 2013, 49, 5390–5392.
- [84] S. Domanski, V. Privman, *J. Phys. Chem. B* 2012, 116, 13690–13695.

- [85] E. Kim, Y. Liu, W. E. Bentley, G. F. Payne, *Adv. Funct. Mater.* **2012**, *22*, 1409–1416.
- [86] M. Zhou, J. Wang, *Electroanalysis* **2012**, *24*, 197–209.
- [87] S. P. Rafael, A. Vallee-Belisle, E. Fabregas, K. Plaxco, G. Palleschi, F. Ricci, *Anal. Chem.* **2012**, *84*, 1076–1082.
- [88] T. K. Tam, *Int. J. Unconventional Computing* **2012**, *8*, 367–381.
- [89] M. Pita, *Int. J. Unconventional Computing* **2012**, *8*, 391–417.
- [90] K. W. Kim, B. C. Kim, H. J. Lee, J. Kim, M. K. Oh, *Electroanalysis* **2011**, *23*, 980–986.
- [91] M. Zhou, F. A. Wang, S. J. Dong, *Electrochim. Acta* **2011**, *56*, 4112–4118.
- [92] M. Zhou, X. L. Zheng, J. Wang, S. J. Dong, *Chem. Eur. J.* **2010**, *16*, 7719–7724.
- [93] E. Richards, *J. Mater. Chem.* **2006**, *16*, C29.
- [94] S. Sivan, S. Tuchman, N. Lotan, *Biosystems* **2003**, *70*, 21–33.
- [95] S. Sivan, N. Lotan, *Biotech. Prog.* **1999**, *15*, 964–970.
- [96] A. Arkin, J. Ross, *Biophys. J.* **1994**, *67*, 560–578.
- [97] G. Strack, M. Pita, M. Ornatska, E. Katz, *ChemBioChem* **2008**, *9*, 1260–1266.
- [98] E. Katz, B. E. Fratto in *Advances in Unconventional Computing* (Ed.: A. Adamatzky), Springer, Amsterdam, **2016**, Vol. 2, Chap. 2, pp. 29–59.
- [99] E. Katz in *Biomolecular Information Processing—From Logic Systems to Smart Sensors and Actuators* (Ed.: E. Katz), Wiley-VCH, Weinheim, **2012**, Chap. 4, pp. 61–80.
- [100] *Methods of Enzymatic Analysis* (Ed.: H.-U. Bergmeyer), Chemie, Weinheim, **1974**.
- [101] J. V. Passonneau, O. H. Lowry, *Enzymatic Analysis: A Practical Guide*, Humana, Totowa, **1993**, Chap. 1, pp. 3–22.
- [102] R. Wilson, A. P. F. Turner, *Biosens. Bioelectron.* **1992**, *7*, 165–185.
- [103] H. B. Dunford in *Peroxidases in Chemistry and Biology*, Vol. 2 (Eds.: J. Everse, K. E. Everse, M. B. Grisham), CRC, Boca Raton, **1991**, pp. 1–24.
- [104] H. Fraga, *Photochem. Photobiol. Sci.* **2008**, *7*, 146–158.
- [105] S. Bakshi, O. Zavalov, J. Halámková, V. Privman, E. Katz, *J. Phys. Chem. B* **2013**, *117*, 9857–9865.
- [106] V. Privman, B. E. Fratto, O. Zavalov, J. Halámková, E. Katz, *J. Phys. Chem. B* **2013**, *117*, 7559–7568.
- [107] J. Halámková, O. Zavalov, L. Halámková, S. Korkmaz, V. Privman, E. Katz, *J. Phys. Chem. B* **2012**, *116*, 4457–4464.
- [108] R. Baron, O. Lioubashevski, E. Katz, T. Niazov, I. Willner, *Org. Biomol. Chem.* **2006**, *4*, 989–991.
- [109] R. Baron, O. Lioubashevski, E. Katz, T. Niazov, I. Willner, *J. Phys. Chem. A* **2006**, *110*, 8548–8553.
- [110] O. Zavalov, V. Bocharova, V. Privman, E. Katz, *J. Phys. Chem. B* **2012**, *116*, 9683–9689.
- [111] J. Zhou, M. A. Arugula, J. Halámková, M. Pita, E. Katz, *J. Phys. Chem. B* **2009**, *113*, 16065–16070.
- [112] J. Halámková, V. Bocharova, M. A. Arugula, G. Strack, V. Privman, E. Katz, *J. Phys. Chem. B* **2011**, *115*, 9838–9845.
- [113] V. Privman, J. Zhou, J. Halámková, E. Katz, *J. Phys. Chem. B* **2010**, *114*, 13601–13608.
- [114] J. Halámková, V. Bocharova, S. Chinnapareddy, J. R. Windmiller, G. Strack, M.-C. Chuang, J. Zhou, P. Santhosh, G. V. Ramirez, M. A. Arugula, J. Wang, E. Katz, *Mol. BioSyst.* **2010**, *6*, 2554–2560.
- [115] M. Pita, M. Krämer, J. Zhou, A. Poghossian, M. J. Schöning, V. M. Fernández, E. Katz, *ACS Nano* **2008**, *2*, 2160–2166.
- [116] M. Pita, J. M. Abad, C. Vaz-Dominguez, C. Briones, E. Mateo-Martí, J. A. Martín-Gago, M. D. P. Morales, V. M. Fernández, *J. Colloid Interface Sci.* **2008**, *321*, 484–492.
- [117] J. Zhao, L. Luo, X. Yang, E. Wang, S. Dong, *Electroanalysis* **1999**, *11*, 1108–1111.
- [118] T. K. Tam, M. Pita, E. Katz, *Sens. Actuators B* **2009**, *140*, 1–4.
- [119] Y. Wang, W. Knoll, *Anal. Chim. Acta* **2006**, *558*, 150–157.
- [120] V. I. Chegel, O. A. Raitman, O. Lioubashevski, Y. Shirshov, E. Katz, I. Willner, *Adv. Mater.* **2002**, *14*, 1549–1553.
- [121] O. A. Raitman, E. Katz, A. F. Bückmann, I. Willner, *J. Am. Chem. Soc.* **2002**, *124*, 6487–6496.
- [122] O. A. Raitman, E. Katz, I. Willner, V. I. Chegel, G. V. Popova, *Angew. Chem. Int. Ed.* **2001**, *40*, 3649–3652; *Angew. Chem.* **2001**, *113*, 3761–3764.
- [123] J. R. Windmiller, P. Santhosh, E. Katz, J. Wang, *Sens. Actuators B* **2011**, *155*, 206–213.
- [124] M.-C. Chuang, J. R. Windmiller, P. Santhosh, G. Valdés-Ramírez, E. Katz, J. Wang, *Chem. Commun.* **2011**, *47*, 3087–3089.
- [125] N. Zhou, J. R. Windmiller, G. V. Ramírez, M. Zhou, J. Halámková, E. Katz, J. Wang, *Anal. Chim. Acta* **2011**, *703*, 94–100.
- [126] N. Guz, T. A. Fedotova, B. E. Fratto, O. Schlesinger, L. Alfonta, D. Kolpashchikov, E. Katz, *ChemPhysChem* **2016**, *17*, 2247–2255.
- [127] S. Mailloux, Y. V. Gerasimova, N. Guz, D. M. Kolpashchikov, E. Katz, *Angew. Chem. Int. Ed.* **2015**, *54*, 6562–6566; *Angew. Chem.* **2015**, *127*, 6662–6666.
- [128] S. Mailloux, N. Guz, A. Zakharchenko, S. Minko, E. Katz, *J. Phys. Chem. B* **2014**, *118*, 6775–6784.
- [129] J. Zhou, T. K. Tam, M. Pita, M. Ornatska, S. Minko, E. Katz, *ACS Appl. Mater. Interfaces* **2009**, *1*, 144–149.
- [130] M. Privman, T. K. Tam, M. Pita, E. Katz, *J. Am. Chem. Soc.* **2009**, *131*, 1314–1321.
- [131] M. Privman, T. K. Tam, V. Bocharova, J. Halámková, J. Wang, E. Katz, *ACS Appl. Mater. Interfaces* **2011**, *3*, 1620–1623.
- [132] E. Katz, S. Minko, *Chem. Commun.* **2015**, *51*, 3493–3500.
- [133] E. Katz, S. Minko, J. Halámková, K. MacVittie, K. Yancey, *Anal. Bioanal. Chem.* **2013**, *405*, 3659–3672.
- [134] X. Yu, W. J. Lian, J. N. Zhang, H. Y. Liu, *Biosens. Bioelectron.* **2016**, *80*, 631–639.
- [135] T. K. Tam, J. Zhou, M. Pita, M. Ornatska, S. Minko, E. Katz, *J. Am. Chem. Soc.* **2008**, *130*, 10888–10889.
- [136] I. Tokarev, V. Gopishetty, J. Zhou, M. Pita, M. Motornov, E. Katz, S. Minko, *ACS Appl. Mater. Interfaces* **2009**, *1*, 532–536.
- [137] M. Motornov, J. Zhou, M. Pita, I. Tokarev, V. Gopishetty, E. Katz, S. Minko, *Small* **2009**, *5*, 817–820.
- [138] E. Katz, A. Poghossian, M. J. Schöning, *Anal. Bioanal. Chem.* **2017** in press DOI: 10.1007/s00216-016-0079-7.
- [139] A. Poghossian, E. Katz, M. J. Schöning, *Chem. Commun.* **2015**, *51*, 6564–6567.
- [140] A. Poghossian, K. Malzahn, M. H. Abouzar, P. Mehndiratta, E. Katz, M. J. Schöning, *Electrochim. Acta* **2011**, *56*, 9661–9665.
- [141] A. Poghossian, M. Krämer, M. H. Abouzar, M. Pita, E. Katz, M. J. Schöning, *Proc. Chem.* **2009**, *1*, 682–685.
- [142] M. Krämer, M. Pita, J. Zhou, M. Ornatska, A. Poghossian, M. J. Schöning, E. Katz, *J. Phys. Chem. C* **2009**, *113*, 2573–2579.
- [143] D. Molinuss, M. Bäcker, H. Iken, A. Poghossian, M. Keusgen, M. J. Schöning, *Phys. Status Solidi A* **2015**, *212*, 1382–1388.
- [144] E. Katz, T. Lötzbecker, D. D. Schlereth, W. Schuhmann, H.-L. Schmidt, *J. Electroanal. Chem.* **1994**, *373*, 189–200.
- [145] I. Willner, G. Arad, E. Katz, *Bioelectrochem. Bioenerg.* **1998**, *44*, 209–214.
- [146] A. Koushanpour, M. Gamella, N. Guz, E. Katz, *Electroanalysis* **2017** in press DOI: 10.1002/elan.201600706.
- [147] T. K. Tam, M. Pita, M. Ornatska, E. Katz, *Bioelectrochemistry* **2009**, *76*, 4–9.
- [148] X. Wang, J. Zhou, T. K. Tam, E. Katz, M. Pita, *Bioelectrochemistry* **2009**, *77*, 69–73.
- [149] V. Bychkova, A. Shvarev, J. Zhou, M. Pita, E. Katz, *Chem. Commun.* **2010**, *46*, 94–96.
- [150] M. Pita, V. Privman, M. A. Arugula, D. Melnikov, V. Bocharova, E. Katz, *Phys. Chem. Chem. Phys.* **2011**, *13*, 4507–4513.
- [151] M. Pita, M. Privman, E. Katz, *Top. Catal.* **2012**, *55*, 1201–1216.
- [152] S. Minko, *J. Macromol. Sci. C* **2006**, *46*, 397–420.
- [153] I. Luzinov, S. Minko, V. V. Tsukruk, *Prog. Polym. Sci.* **2004**, *29*, 635–698.
- [154] M. A. C. Stuart, W. T. S. Huck, J. Genzer, M. Müller, C. Ober, M. Stamm, G. B. Sukhorukov, I. Szleifer, V. V. Tsukruk, M. Urban, F. Winnik, S. Zauscher, I. Luzinov, S. Minko, *Nat. Mater.* **2010**, *9*, 101–113.
- [155] T. K. Tam, M. Pita, M. Motornov, I. Tokarev, S. Minko, E. Katz, *Electroanalysis* **2010**, *22*, 35–40.
- [156] T. K. Tam, M. Pita, M. Motornov, I. Tokarev, S. Minko, E. Katz, *Adv. Mater.* **2010**, *22*, 1863–1866.
- [157] T. K. Tam, M. Pita, O. Trotsenko, M. Motornov, I. Tokarev, J. Halámková, S. Minko, E. Katz, *Langmuir* **2010**, *26*, 4506–4513.
- [158] M. Motornov, T. K. Tam, M. Pita, I. Tokarev, E. Katz, S. Minko, *Nanotechnology* **2009**, *20*, 434006.
- [159] T. K. Tam, M. Ornatska, M. Pita, S. Minko, E. Katz, *J. Phys. Chem. C* **2008**, *112*, 8438–8445.
- [160] V. Bocharova, T. K. Tam, J. Halámková, M. Pita, E. Katz, *Chem. Commun.* **2010**, *46*, 2088–2090.

- [161] M. Motornov, J. Zhou, M. Pita, V. Gopishetty, I. Tokarev, E. Katz, S. Minko, *Nano Lett.* **2008**, *8*, 2993–2997.
- [162] S. Fujii, S. P. Armes, B. P. Binks, R. Murakami, *Langmuir* **2006**, *22*, 6818–6825.
- [163] S. Fujii, E. S. Read, B. P. Binks, S. P. Armes, *Adv. Mater.* **2005**, *17*, 1014–1017.
- [164] B. P. Binks, R. Murakami, S. P. Armes, S. Fujii, *Angew. Chem. Int. Ed.* **2005**, *44*, 4795–4798; *Angew. Chem.* **2005**, *117*, 4873–4876.
- [165] H. W. Duan, D. Y. Wang, N. S. Sobal, M. Giersig, D. G. Kurth, H. Mohwald, *Nano Lett.* **2005**, *5*, 949–952.
- [166] N. Saleh, T. Phenrat, K. Sirk, B. Dufour, J. Ok, T. Sarbu, K. Matyjaszewski, R. D. Tilton, G. V. Lowry, *Nano Lett.* **2005**, *5*, 2489–2494.
- [167] P. P. Konorov, A. M. Yafyasov, V. B. Bogevolnov, *Field Effect in Semiconductor-Electrolyte Interfaces*, Princeton University Press, Princeton, 2006.
- [168] M. W. Shinwari, M. J. Deen, D. Landheer, *Microelectron. Reliab.* **2007**, *47*, 2025–2057.
- [169] Y. G. Vlasov, Y. A. Tarantov, P. V. Bobrov, *Anal. Bioanal. Chem.* **2003**, *376*, 788–796.
- [170] A. S. Poghossian, *Sens. Actuators B* **1992**, *7*, 367–370.
- [171] J. R. Siqueira, M. H. Abouzar, M. Bäcker, V. Zucolotto, A. Poghossian, O. N. Oliveira, M. J. Schöning, *Phys. Status Solidi A* **2009**, *206*, 462–467.
- [172] W. H. Weng, C. W. Wang, S. T. Pang, T. M. Pan, *J. Electrochem. Soc.* **2016**, *163*, B445–B452.
- [173] M. H. Abouzar, A. Poghossian, A. G. Cherstvy, A. M. Pedraza, S. Ingebrandt, M. J. Schöning, *Phys. Status Solidi A* **2012**, *209*, 925–934.
- [174] A. Poghossian, M. Weil, A. G. Cherstvy, M. J. Schöning, *Anal. Bioanal. Chem.* **2013**, *405*, 6425–6436.
- [175] A. Poghossian, M. Bäcker, D. Mayer, M. J. Schöning, *Nanoscale* **2015**, *7*, 1023–1031.
- [176] W. J. Albery, G. J. O’Shea, A. L. Smith, *J. Chem. Soc. Faraday Trans.* **1996**, *92*, 4083–4085.
- [177] A. Lasia in *Electrochemical Impedance Spectroscopy and its Applications*, Springer, New York, 2014, Chap. 10, pp. 251–255.
- [178] M. Munkhjargal, Y. Matsuura, K. Hatayama, K. Miyajima, T. Arakawa, H. Kudo, K. Mitsuabayashi, *Sens. Actuators B* **2013**, *188*, 831–836.
- [179] G. Strack, V. Bocharova, M. A. Arugula, M. Pita, J. Halámek, E. Katz, *J. Phys. Chem. Lett.* **2010**, *1*, 839–843.
- [180] J. Wang, *Nanomachines: Fundamentals and Applications*, Wiley-VCH, Weinheim, 2013.
- [181] J.-F. Morin, *Surface and Solid-State Nanomachines: Preparation, Assembly and Testing*, Wiley-VCH, Weinheim, 2017, in press (ISBN-13: 978-0470592427).
- [182] G. Inzelt, *Conducting Polymers*, Springer, Berlin, Heidelberg, 2008.
- [183] *Handbook of Conducting Polymers* (Eds.: T. A. Skotheim, R. L. Elsenbaumer, J. R. Reynolds), Marcel Dekker, New York, 1998.
- [184] L.-X. Wang, X.-G. Li, Y.-L. Yang, *React. Funct. Polym.* **2001**, *47*, 125–139.
- [185] G. Schopf, G. Koßmehl, *Polythiophenes: Electrically Conductive Polymers*, Springer, Berlin, 1997.
- [186] E. T. Kang, K. G. Neoh, K. L. Tan, *Prog. Polym. Sci.* **1998**, *23*, 277–324.
- [187] R. H. Baughman, *Synth. Met.* **1996**, *78*, 339–353.
- [188] T. F. Otero, J. M. Sansiñena, *Bioelectrochem. Bioenerg.* **1997**, *42*, 117–122.
- [189] T. F. Otero, J. M. Sansiñena, *Bioelectrochem. Bioenerg.* **1995**, *38*, 411–414.
- [190] T. F. Otero, J. M. Sansiñena, *Adv. Mater.* **1998**, *10*, 491–494.
- [191] M. Kaneko, M. Fukui, W. Takashima, K. Kaneto, *Synth. Met.* **1997**, *84*, 795–796.
- [192] Q. Pei, O. Inganläs, *Adv. Mater.* **1992**, *4*, 277–278.
- [193] E. Smela, O. Inganas, I. Lundstrom, *Science* **1995**, *268*, 1735–1738.
- [194] M. Lahav, C. Durkan, R. Gabai, E. Katz, I. Willner, M. E. Welland, *Angew. Chem. Int. Ed.* **2001**, *40*, 4095–4097; *Angew. Chem.* **2001**, *113*, 4219–4221.
- [195] C. Küttel, A. Stemmer, X. Wei, *Sens. Actuators B* **2009**, *141*, 478–484.
- [196] L. Alfonta, A. Bardea, O. Khersonsky, E. Katz, I. Willner, *Biosens. Bioelectron.* **2001**, *16*, 675–687.
- [197] A. Bardea, E. Katz, I. Willner, *Electroanalysis* **2000**, *12*, 1097–1106.
- [198] L. Alfonta, E. Katz, I. Willner, *Anal. Chem.* **2000**, *72*, 927–935.
- [199] F. Patolsky, M. Zayats, E. Katz, I. Willner, *Anal. Chem.* **1999**, *71*, 3171–3180.
- [200] F. Patolsky, E. Katz, A. Bardea, I. Willner, *Langmuir* **1999**, *15*, 3703–3706.
- [201] D. Johannsmann, *The Quartz Crystal Microbalance in Soft Matter Research: Fundamentals and Modeling*, Springer, Heidelberg, 2015.
- [202] A. C. Evans, N. N. Thadani, J. Suh, *J. Controlled Release* **2016**, *240*, 387–393.
- [203] J. Yang, Z. C. Song, S. Liu, Q. Zhang, C. Zhang, *ACS Appl. Mater. Interfaces* **2016**, *8*, 22451–22456.
- [204] D. B. Yao, H. Li, Y. J. Guo, X. Zhou, S. Y. Xiao, H. J. Liang, *Chem. Commun.* **2016**, *52*, 7556–7559.
- [205] *Alginates: Biology and Applications* (Ed.: H. A. Rehm), Springer, Heidelberg, 2009.
- [206] D. Volkov, G. Strack, J. Halámek, E. Katz, I. Sokolov, *Nanotechnology* **2010**, *21*, 145503.
- [207] G. Strack, S. Chinnapareddy, D. Volkov, J. Halámek, M. Pita, I. Sokolov, E. Katz, *J. Phys. Chem. B* **2009**, *113*, 12154–12159.
- [208] M. Pita, L. Cui, R. M. Gaikwad, E. Katz, I. Sokolov, *Nanotechnology* **2008**, *19*, 375502.
- [209] D. Fan, E. Wang, S. Dong, *ACS Appl. Mater. Interfaces* **2017**, *9*, 1322–1330.
- [210] D. Fan, K. Wang, J. Zhu, Y. Xia, Y. Han, Y. Liu, E. Wang, *Chem. Sci.* **2015**, *6*, 1973–1978.
- [211] D. Fan, E. Wang, S. Dong, *Chemical Science* **2017**, *8*, 1888–1895.
- [212] D. Fan, X. Zhu, S. Dong, E. Wang, *ChemPhysChem* **2017**, in press DOI: 10.1002/cphc.201601291.
- [213] S. Liu, M. Li, X. Yu, C.-Z. Li, H. Liu, *Chem. Commun.* **2015**, *51*, 13185–13188.
- [214] L. Halámková, J. Halámek, V. Bocharova, S. Wolf, K. E. Mulier, G. Beilman, J. Wang, E. Katz, *Analyst* **2012**, *137*, 1768–1770.
- [215] J. Zhou, J. Halámek, V. Bocharova, J. Wang, E. Katz, *Talanta* **2011**, *83*, 955–959.
- [216] E. Katz, J. Halámek, *Ann. Forensic Res. Anal.* **2014**, *1*, 1002.

Manuscript received: December 22, 2016

Accepted manuscript online: February 27, 2017

Version of record online: May 2, 2017